www.sciencemag.org/cgi/content/full/330/6006/957/DC1

Supporting Online Material for

Effects of Rapid Global Warming at the Paleocene-Eocene Boundary on Neotropical Vegetation

Carlos Jaramillo,* Diana Ochoa, Lineth Contreras, Mark Pagani, Humberto Carvajal-Ortiz, Lisa M. Pratt, Srinath Krishnan, Agustin Cardona, Millerlandy Romero, Luis Quiroz, Guillermo Rodriguez, Milton J. Rueda, Felipe de la Parra, Sara Morón, Walton Green, German Bayona, Camilo Montes, Oscar Quintero, Rafael Ramirez, Germán Mora, Stefan Schouten, Hermann Bermudez, Rosa Navarrete, Francisco Parra, Mauricio Alvarán, Jose Osorno, James L. Crowley, Victor Valencia, Jeff Vervoort

*To whom correspondence should be addressed. E-mail: jaramilloc@si.edu

Published 12 November 2010, *Science* **330**, 957 (2010)
DOI: 10.1126/science.1193833

This PDF file includes:

Materials and Methods
Figs. S1 to S14
Tables S1 and S5 to S20
References

Other Supporting Online Material for this manuscript includes the following:
available at www.sciencemag.org/cgi/content/full/330/6006/957/DC1

Tables S1 to S4 as a zipped file

Effects of Rapid Global Warming at the Paleocene-Eocene Boundary on Neotropical Vegetation

Carlos Jaramillo, Diana Ochoa, Lineth Contreras, Mark Pagani, Humberto Carvajal-Ortiz, Lisa M. Pratt, Srinath Krishnan, Agustin Cardona, Millerlandy Romero, Luis Quiroz, Guillermo Rodriguez, Milton J. Rueda, Felipe de la Parra, Sara Moron, Walton Green, German Bayona, Camilo Montes, Oscar Quintero, Rafael Ramirez, Germán Mora, Stefan Schouten, Hermann Bermudez, Rosa Navarrete, Francisco Parra, Mauricio Alvarán, Jose Osorno, James L. Crowley, Victor Valencia, Jeff Vervoort.

Supplementary Online Material

Includes methods & expanded results, 14 supplementary figures, and 10 supplementary tables.

1. Statistics

All the analyses, unless noted, were performed using *R for Statistical Computing* (S1), and the packages *Stratigraph* (S2), *Vegan* (S3) and *Cluster* (S4). All comparisons are the result of two-sided t-tests to evaluate the equality of means in two unpaired samples. p is reported for each test at the appropriate point in the text along with degrees of freedom (df) calculated using the Welch modification to account for different variances in the groups being compared.

2. Study Sites and sampling summary

Three sites were studied: Mar 2X, a 450-m-thick sediment core drilled in western Venezuela (11.0601° N, 72.1725° W, paleolatitude = 9.1° N); Riecito Mache, a 600-m-thick outcrop section in western Venezuela (10.7407° N, 72.3664° W, paleolatitude = 8.9° N), and Gonzales, a 170-m-thick outcrop section combined with a 600 m well in northeastern Colombia (8.28° N, 72.57° W, paleolatitude = 6.3° N). The study encompassed 489 carbon isotope samples (Table S1), and 357 palynological samples, recording 37,952 individual occurrences and 1104 morphospecies (Tables S1, S2 and S3). The Mar 2X Core comprised 165 palynological samples, 818 morphospecies and 25,281 occurrences (Table S2); the Riecito Mache section comprised 51 palynological samples, 262 species and 6,069 occurrences (Table S3); and the Gonzales section comprised 141 palynological samples, 244 species and 6,602 occurrences (Table S4). The Mar 2X Core has the highest palynological sample resolution, whereas the other two sites were used to confirm the patterns observed in Mar 2X. The Gonzales outcrop section is from a basin 320 km south of Mar 2x and the Riecito Mache outcrop section is a nearby site, 42 km southwest of Mar 2x.

3. Geology

3.1 Regional Geology

Basin geometries during the Paleogene in Colombia and Venezuela are very complex and do not seem to fit a single model. Studied sections come from two basins:

Catatumbo (Gonzales) and western Maracaibo (Riecito Mache and Mar 2x). Both basins have complicated subsidence histories due to eustatic and tectonic regimes that changed through time.

Catatumbo basin (Santander and craton-derived sediments). The basin sediments were derived from the Santander Massif, Merida Arch and the South American craton; the depositional systems prograde toward the Maracaibo Gulf (S5,S6). The regional progradation during the late Maastrichtian to late Paleocene is associated with the uplift of western massifs. A drop of base level due to a decrease in tectonic subsidence produced a sequence boundary during the late early Eocene, followed by coarse-grained fluvial deposition during the middle Eocene. Then, uplift of nearby western blocks led to the filling of a foredeep basin during the late Eocene to early Oligocene. Paleogene sediments are fully fluvial and there is no evidence of major time hiatuses (S5,S7,S8,S9).

Westernmost Maracaibo basin. The Paleocene-Lower Eocene succession in this area changes upsection, from carbonates with terrigenous material of the Guasare Formation to coal-bearing mudstone and sandstones of the Marcelina Formation. Overlying it are sandstones, mudstones, and conglomerate beds of the Misoa and Mostrencos Formations. In some areas toward the east of Maracaibo, the Misoa rests unconformably on top of the Marcelina, whereas there is no hiatus to the west (S5,S10,S11). This succession records syn-orogenic filling of a shallow marine basin that has progradational clastic wedge with source areas located to the west. The thin succession reported in this paper is at the lower segment of the Mostrencos Formation (Riecito Mache) and the middle segment of the Marcelina Formation (Mar 2x).

3.2. Lithological Description of the Sections

The PETM was identified at the middle Marcelina Formation in Mar 2x, at the lower Mostrencos Formation in Riecito Mache and at the upper Cuervos Formation in Gonzales. The Marcelina and lower Mostrencos Formations were accumulated in coastal plain deposits, whereas the Cuervos Formation was accumulated in fluvial deposits.

3.2.1 Mar 2x

The studied interval of the Mar 2x core (Fig. S1) consists of the middle part of the Marcelina Formation that contains the PETM. The sequence is characterized by cross-bedded sandstone with shale and coal interbeddings, forming fining-upward intervals, up to 20 m-thick. This unit is interpreted as coastal and delta plain channels and associated overbank environments. Towards the top of the core (upper Marcelina) intercalated shale and ripple cross-laminated and bioturbated sandstone are more common, recording coastal and interdistributary bay and delta front environments. Lithological description was complemented by information provided by Petroleos of Venezuela-PDVSA (S12).

3.2.2 Riecito Mache

The sequence measured in the Riecito Mache section (Figs. S2-3) corresponds to the Paso Diablo and Mostrencos Formations. The Paso Diablo Formation consists of shale and coal with lenticular and tabular sandstone interbeddings, and cross-bedded sandstone with an erosive base forming fining-upward intervals up to 4 m thick. This unit was deposited in delta plain environments. The Mostrencos Formation contains cross-bedded sandstone with conglomeratic lenses, forming fining-upward intervals up to 15-m-thick, intercalated with shale and coal, and locally with tuffaceous sandstone. This unit is interpreted to represent low-sinuosity coastal plain environments. The PETM lies within the lower Mostrencos Formation. The section described herein was combined with a description and sampling of the same section conducted in the 1950's by H.W. Steckhoven (Royal Shell). Samples from the Steckhoven column, which were stored along with the stratigraphic column at the Core Library of PDVSA in Maracaibo, were analyzed by Rull (S11). His work showed a gradual increase in diversity from the Paleocene into the early Eocene. However, his study was based only on key biostratigraphic taxa, thus excluding a large number of taxa. Even with this biased data collection, Rull's analysis reached the same conclusion as ours, i.e. there is a gradual transition in the vegetation and increasing diversity in the Early Eocene.

3.2.3 Gonzales

An outcrop section and a well drilled at the outcrop section were used in this study (Figs. S4 and S5). The correlation of the outcrop section and the well is straightforward (see correlation points in Fig. S5). All samples for the analysis were expressed in units of the Gonzales well, because it had a more complete section. The upper segment of the Cuervos Formation, the segment containing the PETM, is characterized by fine-grained successions interbedded with meter-scale channel-fill sandstones that record fluvial deposition in a basin with high subsidence.

4. Identifying the PETM interval

We have three independent lines of evidences indicating the PETM interval in the different sections.

1) Radiometric dating. Within the upper part of the PETM interval in Riecito Mache, a radiometric age of 56.09+ 0.03 Ma was determined using a high-resolution technique (Chemical Abrasion– Thermal Ionization Mass Spectrometry). This age is within one of the possible ages estimated for the PETM (S13); given a duration of ~200K for the PETM, its age would span from 56.33 to 56.13.

2) Biostratigraphic dating. Palynostratigraphy has been used in the region over the last 50 years as the main biostratigraphic tool by numerous oil companies and researchers. There are several taxa indicators for both the onset of the Eocene and the end of the Paleocene. Within the PETM interval, there are 10 key Eocene taxa originating and 3 key Paleocene taxa becoming extinct. This co-occurrence of events happens in all three sections (Mar 2x, Riecito Mache, and Gonzales). In summary, there is a strong biostratigraphic support for the PETM position.

3) The Carbon Isotope record, both in Bulk and compound specific carbon isotope records. Bulk isotope records of all cores indicate that PETM interval samples have a statistically lower bulk $\delta^{13}C$ values than late Paleocene samples (1.7 to 1.9‰). The bulk carbon isotope records from our sections are noisier as compared to carbon isotope record obtained from carbonates of deep-water sediments, likely because several factors, other than the atmospheric values of $\delta^{13}C$, influence the $\delta^{13}C$ signal in a fluvial setting (S14). However, in spite of all possible biases, PETM interval has a statistically significant lower bulk $\delta^{13}C$ values than late Paleocene samples (1.7 ‰). This difference is the same value (1.7 ‰) of the difference between the mean value of PETM samples versus late Paleocene samples that is found in Wyoming (S15), the best studied PETM terrestrial site in the world. When the most negative sample found within the PETM is compared with the Late Paleocene (e.g., the peak of the carbon excursion), the PETM excursion in our sites (2.9 to 3.2‰) is lower than in Wyoming (3.8‰) (S15), that could indicate that we

are missing the peak of the excursion. We measured $\delta^{13}C$ on *n*-alkanes in the Mar2x core, which targets vascular plants material only. The results show that the *n*-alkanes confirm the bulk isotope records and show a negative carbon isotope excursion in all odd carbon numbered *n*-alkanes measured and ranges between 2-3‰.

In conclusion, these three independent lines of evidence indicate all sections contain the PETM interval. In the following headings (4.1, 4.2 and 4.3), we expand on the explanation of each line of evidence.

4.1. Radiometric Dating (U-Pb Zircon Geochronology)

A first order dating of the PETM worldwide has remained elusive due to the absence of associated volcanic material. The PETM was dated by establishing its position relative to dated ash -17 that lies within magnetochron C24r (S16).

In Riecito Mache an intercalated felsic pyroclastic tuff was dated using TIMS (Chemical Abrasion– Thermal Ionization Mass Spectrometry) to 56.09+ 0.03 Ma. This volcanism is linked to the northern Andes and Circum-Caribbean Paleogene magmatic province (S17,S18). The volcanic layer was found within the PETM, at meter 1290, which is 11 m below the top the PETM (at 1301 m), and 67 meters above the bottom of the PETM (at 1223 m). The age of the onset of the PETM can be estimated with our new date if sedimentation is assumed constant during this interval and the duration is between 170 kyr (S19) and 220 kyr (S20). The PETM onset is estimated at 56.24 Ma (assuming 170 kyr) to 56.28 Ma (assuming 220 kyr). This range is closest to the orbital cyclostratigraphy option 3 (56.33 Ma) for the age of the PETM onset (S16).

Due to the common existence of older zircon crystals within explosive volcanics, either as reworked grains from previous volcanic phases or as inherited zircons associated with melting of older crust (S21,S22), two U-Pb geochronological methods were used to constrain the age of the youngest zircon in the Riecito Mache tuff, which is interpreted as having formed during eruption. Zircons were mounted in epoxy, polished, and examined by cathodoluminescence imaging to reveal the internal structure. Only grains with a simple growth history that appeared to indicate a single-stage crystallization were analyzed. Forty-eight grains in the epoxy mount were analyzed using LA-ICP-MS (laser ablation inductively coupled plasma mass spectrometry) at Washington State University.

Thirty-two grains were identified as being part of the youngest population, ten of which were removed from the epoxy mount and analyzed by the more precise CA-TIMS (chemical abrasion thermal ionization mass spectrometry) method at Boise State University.

Due to the greater precision, we use the CA-TIMS results for our age interpretations. The $^{206}Pb/^{238}U$ dates from the six youngest grains are equivalent with a weighted mean of 56.09 ± 0.03 Ma (MSWD = 1.5, Fig. S6, Table S5, calculated with Isoplot 3.0 (S23)), which is interpreted as the eruption age of the Riecito Mache tuff. The error is the internal error based on analytical uncertainties only, including counting statistics, instrumental fractionation, subtraction of tracer solution, and blank and initial common Pb subtraction. It is the 2σ error expanded by the square root of the MSWD and the Student's T multiplier of n-1 degrees of freedom. This error should be considered when comparing our date with $^{206}Pb/^{238}U$ dates obtained by other laboratories with tracer solutions that were similarly calibrated using EARTHTIME gravimetric standards. When comparing our date with those derived from other decay schemes (e.g., $^{40}Ar/^{39}Ar$, $^{187}Re-^{187}Os$), systematic uncertainties in the tracer calibration and ^{238}U decay constant (S24) should be added to the internal error in quadrature. This error is ± 0.13 Ma. Errors on the individual analyses are 2σ internal errors based on analytical uncertainties only.

Three other grains yielded slightly older CA-TIMS $^{206}Pb/^{238}U$ dates of 56.39 ± 0.04 to 56.17 ± 0.04 Ma, and one other grain yielded a significantly older date of 67.5 ± 0.1 Ma. The older analyses are interpreted as being from grains that had prolonged magma residence or contained inherited cores

4.1.1 U-Pb LA-ICPMS

Heavy mineral concentrates of the <350 μm fraction were separated magnetically. Inclusion-free zircons from the non-magnetic fraction were then handpicked under a binocular microscope. Fifty zircons were mounted in epoxy and polished to half thickness for laser ablation analyses, using laser ablation–inductively coupled plasma–mass spectrometry. All LA-ICP-MS U-Pb analyses were conducted at Washington State University using a New Wave Nd:YAG UV 213-nm laser coupled to a ThermoFinnigan Element 2 single collector, double-focusing, magnetic sector ICP-MS. Operating procedures and parameters are discussed in greater depth by Chang et al. (S25) and are only briefly outlined here. Laser spot size and repetition rate were 30 nm and 10 Hz, respectively. He and Ar carrier gases delivered the sample aerosol to the plasma. Each analysis consisted of a short blank analysis followed by 300 sweeps through masses 204, 206, 207, 208, 232, 235, and 238, taking approximately 35 seconds.

LA-ICP-MS isotopic analyses are affected by two forms of inter-element fractionation that must be corrected (S26). Time-dependent fractionation results from the more efficient volatilization of Pb over U as the laser excavates successively deeper levels in the ablation pit during an analysis, which in turn leads to an increase in $^{206}Pb/^{238}U$ and $^{207}Pb/^{235}U$ ratios with time (S27). It has been demonstrated that U/Pb fractionation is approximately linear over the short time interval of the analysis (S26). By definition, time-dependent fractionation is zero at the beginning of the analysis. Regression of time series data to the intercept at $t = 0$, therefore, yields the point at which time- dependent fractionation equals zero.

Time-independent (or static) fractionation is the largest source of uncertainty in LA-ICP-MS U-Pb geochronology and results from mass and elemental static fractionation in the plasma and also poorly understood laser-matrix effects (S26). The time-independent fractionation corrected by normalizing U/Pb and Pb/Pb ratios of the unknowns to the zircon standards (S25). For this study we used two zircon standards: Peixe, with an age of 564 Ma (S28), and FC-1, with an age of 1099 Ma (S29). Peixe was used to correct the $^{238}U/^{206}Pb$ and $^{235}U/^{207}Pb$ ratios and FC-1 was used to correct the $^{207}Pb/^{206}Pb$ ratios.

Common Pb can represent a proportionally large contribution to the total Pb in Mesozoic and younger U-poor zircons. However, common Pb is typically not significant in LA-ICP-MS analyses, most likely because it is concentrated in cracks and inclusions, which can be avoided. When this is not possible, the influence of common Pb is easy to recognize on Tera-Wasserburg diagrams because analyses tend to line up on a steep linear trajectory that can be anchored at a reasonable $^{207}Pb/^{206}Pb$ common lead composition (y-intercept) (S30). Common Pb corrections were made on these analyses using the ^{207}Pb method (S31). The U-Pb age was calculated using Isoplot (S23). The final crystallization ages that we report are using the algorithm of TUFFZIRC. Analyses that are statistically excluded from the main cluster are shown in gray on the figure. The ages that we report in Table S6 are at the one sigma level and report only analytical error. The final age error (Table S6) was calculated using two uncertainties: the first is derived from the uncertainty of the TUFFZIRC age calculation alone, and the second represents the systematic uncertainty during that session (~1.1 %). The age uncertainty is determined as the quadratic sum of the TUFFZIRC error plus the total systematic error for the set of analyses (~1.2%). The obtained TUFFZIRC age of 55.8 ± 0.7 overlaps within error with the CA-TIMS age (Figure S7).

4.1.2 U-Pb CA-TIMS

From the major youngest population of zircon that were identified during LA-ICPMS analysis, which we interpreted as having formed during eruption of the tuff, ten single zircon analyses were selected for chemical abrasion–thermal ionization mass spectrometry (CA-TIMS) at Boise State University.

Zircons were subjected to a modified version of the chemical abrasion method of Mattinson (S32), reflecting analysis of single grains. Grains were removed from epoxy mounts after LA-ICPMS dating and cathodoluminescence imaging, and then placed in a muffle furnace at 900°C for 60 hours in quartz beakers. Single grains were then transferred to 3 ml Teflon PFA beakers and loaded into 300 µl Teflon PFA microcapsules. Fifteen microcapsules were placed in a large-capacity Parr vessel, and the crystals were partially dissolved in 120 µl of 29 M HF for 12 hours at 180°C. The contents of each microcapsule were returned to 3 ml Teflon PFA beakers, the HF removed and the residual grains were immersed in 3.5 M HNO_3, ultrasonically cleaned for an hour, and fluxed on a hotplate at 80°C for an hour. The HNO_3 was removed and the grains were rinsed twice in ultrapure H_2O before being reloaded into the same 300 µl Teflon PFA microcapsules (rinsed and fluxed in 6 M HCl during sonication and washing of the grains) and spiked with the Boise State University mixed ^{233}U-^{235}U-^{205}Pb tracer solution. These chemically abraded grains were dissolved in Parr vessels in 120 µl of 29 M HF with a trace of 3.5 M HNO_3 at 220°C for 48 hours, dried to fluorides, and then re-dissolved in 6 M HCl at 180°C overnight. U and Pb were separated from the zircon matrix using an HCl-based anion-exchange chromatographic procedure (S33), eluted together and dried with 2 µl of 0.05 N H_3PO_4.

Pb and U were loaded on a single outgassed Re filament in 5 µl of a silica-gel/phosphoric acid mixture (S34), and U and Pb isotopic measurements made on a GV Isoprobe-T multicollector thermal ionization mass spectrometer equipped with an ion-counting Daly detector. Pb isotopes were measured by peak-jumping all isotopes on the Daly detector for 100 to 160 cycles, and corrected for 0.15 ± 0.06%/a.m.u. (2σ) mass fractionation. Transitory isobaric interferences due to high-molecular weight organics, particularly on ^{204}Pb and ^{207}Pb, disappeared within approximately 30 cycles, ionization efficiency averaged 104 cps/pg of each Pb isotope. Linearity (to ≥1.4 x 10^6 cps) and the associated deadtime correction of the Daly detector were monitored by repeated analyses of NBS982, and have been constant since installation. Uranium was analyzed as UO^{2+} ions in static Faraday mode on 10^{11} ohm resistors for 200 to 250 cycles, and corrected for isobaric interference of $^{233}U^{18}O^{16}O$ on $^{235}U^{16}O^{16}O$ with an $^{18}O/^{16}O$ of 0.00206. Ionization efficiency averaged 20 mV/ng of each U isotope. U mass fractionation was corrected using the known $^{233}U/^{235}U$ ratio of the tracer solution.

U-Pb dates and uncertainties were calculated using the algorithms of Schmitz and Schoene (S35), $^{235}U/^{205}Pb$ of 77.93 and $^{233}U/^{235}U$ of 1.007066 for the Boise State University tracer solution, and U decay constants recommended by Jaffey et al. (S24). $^{206}Pb/^{238}U$ ratios and dates were corrected for initial ^{230}Th disequilibrium using a Th/U[magma] = 3 using the algorithms of Crowley et al. (S36), resulting in an increase in the $^{206}Pb/^{238}U$ dates of ~0.09 Ma. All common Pb in analyses was attributed to laboratory blank and subtracted based on the measured laboratory Pb isotopic composition and associated uncertainty. U blanks are difficult to precisely measure, but are estimated at 0.07 pg.

4.2. Biostratigraphic Datums

Palynology has been used extensively as a biostratigraphic tool in Colombia and Venezuela over the past 50 years, mainly by the oil industry, with excellent results (S37,S38,S39,S40,S41,S42,S43). In Mar 2x, within the PETM, there is the last appearance datum (LAD) of three key Paleocene markers (S38,S39,S42,S44), *Foveotricolpites perforatus* (2310.6 m or 7580.6 ft), *Bombacacidites annae* (2287.6 m or 7505.3 ft), and *Retidiporites magdalenensis* (2310.6 m or 7580.6 ft), as well as the first appearance datum (FAD) of several Eocene markers (S38,S39,S42,S44) including *Cyclusphaera scabrata* (2314.7 m or 7594.4 ft), *Rhoipites hispidus* (2308.9 m or 7575.2 ft), *Retitrescolpites*? *irregularis* (2316.8 m or 7601.3 ft), *Tetracolporopollenites transversalis* (2315.5 m or 7596.9 ft), *Margocolporites vanwijhei* (2287.6 m or 7505.3 ft), *Tetracolporopollenites maculosus* (2294.2 m or 7527 ft), *Retibrevitricolpites triangulatus* (2316.8 m or 7601.3 ft), *Racemonocolpites facilis* (2311.1 m or 7582.5 ft), *Corsinipollenites undulatus* (2294.2 m or 7527 ft), and *Psilastephanocolporites fissilis* (2311.1 m or 7582.5 ft). Depths are given in both meters and feet, as the Mar2x core was taken using the English system, commonly used in the oil industry.

Biostratigraphy also confirms the position of the PETM in Riecito Mache (the LAD of *Foveotricolpites perforatus* 1261 m, *Bombacacidites annae* 1261 m, *Retidiporites magdalenensis* 1232 m, and the FAD of *Cyclusphaera scabrata* 1229.75 m, *Retitrescolpites? irregularis* 1229.75 m, *Tetracolporopollenites transversalis* 1229.75 m, *Margocolporites vanwijhei* 1295.45 m, *Retibrevitricolpites triangulatus* 1229.75 m, *Striatopollis catatumbus* 1229.78 m, *Ranunculacidites operculatus* 1295.45 m, *Rhoipites guianensis* 1281.8 m). Biostratigraphy also confirms the PETM in Gonzales (LAD of *Bombacacidites annae* (246.8 m or 810ft) and the FAD of *Cyclusphaera scabrata* (227.8 m or 747.4 ft), *Rhoipites hispidus* (226.3 m or 742.5 ft), *Racemonocolpites facilis* (223.5m or 733.5 ft), and *Rhoipites guianensis* (227.35 m or 745.9 ft).

The Paleocene/Eocene boundary is defined by the Carbon Isotope Excursion (CIE), which lies within the lower part of planktonic foraminifera zone P5 (*Morozovella velascoensis*) of Berggren et al. 2005 (S45,S46). Dating terrestrial strata in tropical South America traditionally has been done with palynology (S38,S40,S42,S47,S48,S49). The calibration of these palynological zones to the geological time scale has been developed over many years and it is not an easy task. Researchers, mostly from the oil industry, have been able to analyze marine cores that have terrestrial palynomorphs, in order to calibrate the palynological zones (S38,S42). Additionally, the long-term record of $\delta^{13}C$ has been used as a calibration tool (S50,S51). The upper part of palynological zone *Retidiporites magdalenensis* of Germeraad et al. (S38), which contains the taxa used here to indicate the late Paleocene (as described above) has been calibrated to planktonic foraminifera zone P4 of Berggren et al. (S45) by the co-ocurrence of *Globorotalia pseudomenardii* and *Morozovella velascoensis* (S38). Zone P4 is dated as late Paleocene (S46). Palynological zone *Retibrevitricolporites triangulatus* of Germeraad et al. (S38), which contains the taxa used here to indicate the early Eocene (as described above), has been calibrated to planktonic foraminifera zone P5 of Berggren (S45) by the occurrence of *Morozovella velascoensis* and the absence of *Globorotalia pseudomenardii* (S38). Zone P5 as been dated as early Eocene to latest Paleocene (S46). The comparison of the long-term global $\delta^{13}C$ record of Zachos et al. (S52) to the Maastrichtian to middle Eocene record of the $\delta^{13}C$ in strata from Colombia has also been used to calibrate the palynological zones of the Paleogene of Colombia (S50,S51). The exact relationship of the palynological zones with the Paleocene/Eocene boundary (the PETM) has never been studied in detail. In this study we found that the transition from the *Retidiporites magdalenensis* to the *Retibrevitricolporites triangulatus* zone happens within the PETM interval, as confirmed by the radiometric dating.

4.3 Stable carbon isotopes

4.3.1 Bulk Carbon Isotopic Analysis

Stable carbon-isotope values of bulk organic matter (δ^{13}CTOM) were measured via flash-pyrolysis at 1100 °C in a Costech elemental analyzer fitted to a Thermo Finnigan Delta plusXP isotope ratio mass spectrometer (Department of Geological Sciences at Indiana University-Bloomington). Carbonate present in the samples was removed by HCl digestion. Analytical precision and accuracy were determined on the basis of repeated analysis of two internal lab standards calibrated against the internationally accepted V-PDB standard. Overall uncertainty was better than 0.08‰. Organic carbon content (TOC) was determined on the basis of the liberated CO_2 in the elemental analyzer. $\delta^{13}C$ values are given in Table S1.

Bulk organic $\delta^{13}C$ values of Mar 2x were also complemented by a Middle to Late Paleocene record of $\delta^{13}C$ in a nearby core, 58 km to the west (S53). The PETM was identified in the 2287–2322 m interval. $\delta^{13}C$ values of the PETM are significantly more negative than that of the Middle-Late Paleocene (mean -27.3‰ vs. -25.6‰, $p < 0.0002$, df: 104.556), and slightly more negative than the $\delta^{13}C$ of the earliest Eocene (-27.1), although the difference is not significant ($p < 0.193$, df: 110.82). At Riecito Mache, the PETM is contained within 1223-1301 m interval [PETM -27.4, Paleocene -25.7, $p < 0.001$, df: 7.799; Early Eocene -26.2, $p < 0.005$, df: 7.824]. At Gonzales, the PETM is contained within 222.5- 251.5 m interval [PETM -27.4‰, Paleocene -25.5‰, $p < 0.001$, df: 32.849; Early Eocene -24.9‰, $p < 0.001$, df: 25.473]. The most negative isotope value within the PETM compared to late Paleocene values (e.g., the peak of isotope excursion) is 2.92‰ at 2293.6 m in Mar 2x, 3.2‰ at 1231.5 m in Riecito Mache, and 3.04‰ at 227.3 m in Gonzales.

Because $\delta^{13}C$ values of bulk sediments can be affected by the total organic carbon of a sample (S15); we applied the Wing residuals method (S15) to the $\delta^{13}C$ record of the three sites. The resulting pattern does not differ significantly from the raw data (Figs. S8, S9, S10).

4.3.2. Plant Biomarkers

Sediments were extracted with 2:1 (v/v) dichloromethane: methanol using an accelerated solvent extractor (ASE 300; Dionex Corporation) at $120^{0}C$, 1,500 p.s.i., for 25 minutes. Lipid fractions were separated by silica gel column chromatography using an elution sequence of hexane, dichloromethane, and methanol. Cyclic and branched alkanes were separated from normal and isoalkanes by urea adduction. The hydrocarbon fraction (hexane fraction) was dried under a stream of N_2 and dissolved in a mixture of methanol-saturated urea, pentane and acetone (200ul each). The resulting urea crystals were extracted with hexane yielding cyclic/branched alkanes. Remaining crystals are dissolved in 1:1 (v/v) H_2O: methanol, then extracted with hexane to yield the *n*-alkane fraction. We also performed silver nitrate impregnated silicagel chromatography as an additional clean-up step before compound specific isotopic analysis. For *n*-alkane analysis, low values of Carbon Preference Index (CPI; $\sum(C_{25}+C_{27}+C_{29}+C_{31})/\sum(C_{24}+C_{26}+C_{28}+C_{30})$ were used to eliminate samples that could be biased by contributions from other marine sources such as aquatic plants. All samples with a CPI value less than 1.38 were not used for isotopic analysis.

The *n*-alkane fraction was analyzed for stable carbon and hydrogen isotopic compositions on a Thermo Finnigan MAT 253 mass spectrometer interfaced with a Thermo Finnigan Trace GC Combustion III (for carbon) and High Temperature Conversion (for hydrogen) systems. A J&W Scientific DB-1 capillary column was used to separate individual n-alkanes. Temperature was programmed from 60°C (held for 1 min) at 6°C min^{-1} to 320°C and held for 25 min isothermally. A programmed temperature vaporizing injector was used with Helium as a carrier gas with a column flow rate of 2.0 ml min^{-1}. Carbon isotopic compositions are expressed relative to VPDB standard. The analytical accuracy and precision are determined based on repeated analysis of a standard n-alkane mixture (MixB2 containing C16-C30 n-alkanes; isotopic ratios measured offline by A. Schimmelmann, Biogeochemical Laboratories, Indiana University). The standard error of n-alkane $\delta^{13}C$ (based on duplicates of n samples) was ±0.8‰ or better. H_2 was obtained from organic hydrogen by pyrolytic conversion at 1400°C. The H_3^+ factor (proportionality constant between the concentration of H_2 and H_3^+) was determined daily using reference H_2 gas. Analytical accuracy and precision of the system were determined using the mixture of n-alkane compounds. Standard error was generally less than ±5‰. Results are summarized in Table S7, Figure S11 (C n-alkane), and Figure S12 (D n-alkane).

5. Diversity Analyses

Pollen and spore morphotypes reflect mostly generic diversity (S38) with some few types reflecting diversity at the species and family levels, although the natural affinity of many of the morphotypes in our database is still unknown. However, there is no reason to expect a systematic bias in the taxonomic representation of the pollen or spores that would affect any segment of the diversity pattern. Palynological data have been previously used to study plant diversity over different time scales (S54,S55,S56,S57,S58,S59,S60,S61).

Species morphologies can be seen in our online morphological database at http://biogeodb.stri.si.edu/jaramillo/palynomorph/. An additional 390 Mb Filemaker file with photos and descriptions can be downloaded from the Smithsonian Tropical Research Institute Data Repository at http://biogeodb.stri.si.edu/jaramillo/paper/paperData.html The raw abundance counts for each of the sites are given in Tables S2, S3, and S4.

5.1 Standing Diversity

We used the range-through method to calculate standing diversity, because it decreases the bias produced by changes in facies and depositional environments (Table S8). All species with single occurrences were eliminated from the standing diversity analysis. Standing diversity was not calculated for Gonzales because samples of the PETM interval had higher counts than both Eocene and Paleocene samples (counts of 111.1 vs. 259.6, $p < 0.001$), and higher sample counts artificially increase standing diversity.

5.2 Piecewise Analysis

The edge effect (S62) in the standing diversity curve was estimated using a piecewise regression. This regression assumes that there are two different regression functions to the same data (S63) and attempts a two-segment fit of the data. The breakpoint is the intersection of the two fitted regression lines. The regression iteratively tries all possible positions of the breakpoint and chooses the one that produces the lowest residual sum of squares (S64). The model to fit follows the algorithm described by Duggleby and Ward (S65) for a two-segment linear regression: $y = y_T + [(m_L + m_R)(x - x_T) - (m_L - m_R)\,|x - x_T|\,] / 2$ y= FAD or LAD, x = species, x_T = breakpoint species, y_T = breakpoint FAD or LAD, m_L = slope left of breakpoint, m_R = slope right of breakpoint. Following is the code used in R and the package *Stratigraph* to perform the analysis.

```
##FAD EDGE
mar2x.edge=strat.column(counts=t(mar2x.countsNoSingles),depths=mar2x.depthFeet,sa
mple.labels=mar2x.Species)#Singles out
mar2x.FAD=fads(mar2x.edge)#FAD, singles excluded
mar2x.LAD=lads(mar2x.edge)#LAD, singles excluded

fad.edge<-mar2x.FAD[which(mar2x.FAD>7400)]##time restricted to edge effect for
FAD, up to 64My
fad.edge<-sort(fad.edge,decreasing = TRUE)##fad arranged from oldest to youngest
span=length(fad.edge)#length of the analysis, to be included in the next line
cumuedge.fad<-c(1:span)
step1<-numeric(span)##first segment of piecewise
for (i in (1:span)){
```

```
step1[i]<-sum(resid(lm(fad.edge[1:i]~cumuedge.fad[1:i]))^2)
}
step2<-numeric(span)##last segment of piecewise
for (i in (1:span)){
step2[i]<-sum(resid(lm(fad.edge[i:span]~cumuedge.fad[i:span]))^2)
}
piecewise<-step1+step2## sum of first and second segment
breakpoint=which(piecewise==min(piecewise))## the position of the minimum value,
data 148
fad.edge[breakpoint]##7698.1  Ma

##LAD EDGE
mar2x.edge=strat.column(counts=t(mar2x.countsNoSingles),depths=mar2x.depthFeet,sa
mple.labels=mar2x.Species)
mar2x.FAD=fads(mar2x.edge)#FAD, singles excluded
mar2x.LAD=lads(mar2x.edge)#LAD, singles excluded

lad.edge<-mar2x.LAD[which(mar2x.LAD<7400)]##time restricted to edge effect for
FAD, up to 64My
lad.edge<-sort(lad.edge)##lad arranged from youngest to oldest
span=length(lad.edge)#length of the analysis, to be included in the next line
cumuedge.lad<-c(1:span)
step1<-numeric(span)##first segment of piecewise
for (i in (1:span)){
step1[i]<-sum(resid(lm(lad.edge[1:i]~cumuedge.lad[1:i]))^2)
}
step2<-numeric(span)##last segment of piecewise
for (i in (1:span)){
step2[i]<-sum(resid(lm(lad.edge[i:span]~cumuedge.lad[i:span]))^2)
}
piecewise<-step1+step2## sum of first and second segment
breakpoint=which(piecewise==min(piecewise))## the position of the minimum value,
data 148
lad.edge[breakpoint]##6986.1
```

5.3 DCA Analysis

A Detrended Correspondence Analysis (DCA) (S66) was performed, using the function *decorana* from the package VEGAN. The DCA was performed on the composite section after the range-through assumption. Singletons were excluded.

5.4 Cluster Analysis

An agglomerative cluster analysis (S67), using Euclidean distance, was performed using the function *agnes* from the package *Cluster*. The Cluster was performed on the composite section after the range-through assumption. Singletons were excluded. The agglomerative coefficient, which measures the amount of clustering structure found, was 0.8761647 for Mar 2x, 0.7975151 for Riecito Mache, and 0.7949479 for Gonzales (Fig. S13).

5.5 Within-Sample Diversity (Rarefaction)

The within-sample diversity was analyzed using rarefaction (S68). The number of morphotypes found at counts of 100, 120 and 150 grains was calculated for each sample, using the package VEGAN (Table S8). In Gonzales, at 100-counts, the Paleocene is lower than the PETM (12.5 vs. 18.1, $p < 0.06$, *df : 5.04*), and the PETM is lower than the Eocene (18.1 vs. 26.2, $p < 0.07$, *df: 7.123*). In Riecito Mache, rarefaction was not calculated because very few samples had counts greater than 100 grains.

5.6 Simpson Index

The Simpson Index (S69) was calculated using *Stratigraph,* and performed in samples with a count above 80 grains (Table S8). In Riecito Mache, the Paleocene (0.74) is slightly lower than the PETM (0.76), $p < 0.82$, *df: 7.9*. One PETM sample (depth 1223) has the lowest Simpson value (0.2), much lower that all other samples of either the Paleocene or the PETM, and it is almost fully dominated by the species *Proxapertites "minutihumbertoides"*. If this sample is removed from the comparison, the Paleocene (0.74) is lower than the PETM (0.81), although the difference is not significant ($p < 0.503$, *df: 5.9*). In Gonzales, the Paleocene (0.57) is lower than the PETM (0.79, $p < 0.001$, *df: 19.148*), and the PETM is lower than the early Eocene (0.88, $p < 0.016$, *df: 11.9*).

5.7 Angiosperms and Ferns

Only samples with counts greater than 80 grains are considered in this analysis. In Mar 2x, angiosperm relative abundance is lower in the Paleocene (76.8%) than in the PETM (84.6%; $p < 0.07$, df: 37.7), whereas it is similar in the PETM and Eocene (86.9%; $p < 0.28$, df: 24.03). Angiosperm standing diversity is lower in the Paleocene

(136.36) than in the PETM (165.1, $p < 0.001$, df: 28.34), which itself has lower diversity than the Eocene (190.4, $p < 0.001$, df: 25.06). Fern spore standing diversity, on the other hand, does not change from the Paleocene (37.2) to the PETM (37.5; $p < 0.74$, df: 35.5), but it does increase slightly in the Eocene (40.4) ($p < 0.0001$, df: 27.7). This pattern is also seen in Gonzales and Riecito Mache.

In Riecito Mache, relative abundance of spores does not significantly change across the PETM (16.7 in Paleocene, 8.4 in PETM, $p < 0.5317$, df: 4.794), nor does that of pollen (Paleocene = 83.2 vs. Eocene = 91.5, $p < 0.531$, df: 4.7). Spore standing diversity is lower in the Paleocene (19.5) than in the Eocene (22.3), $p < 0.015$, df: 19.7, as well as pollen standing diversity [Eocene (72.8). Paleocene (56.8), $p < 0.0001$, df: 14.7].

In Gonzales, spore relative abundance slightly decreases from the Paleocene (29.5) to the Eocene (5.8, $p < 0.0001$, df = 54.); angiosperm pollen also increases in abundance (71.8 vs. 94.9). Spore standing diversity (after range-through) does not change from the Paleocene to the Eocene (12.6 vs. 12.5 , $p < 0.87$, df: 26.1). Angiosperm pollen became more diverse in the Eocene compared to the Paleocene (54.8 vs. 80.8, $p < 0.0001$, df: 23.4).

5.8 Floristic Affinities

Floristic affinities were determined from the following sources: (S9,S38,S40,S41,S47,S48,S49,S70,S71,S72,S73,S74,S75,S76,S77,S78). In the following list we specified the natural affinities of the taxa, grouped by Family, which we used in the analysis.

Arecaceae
Arecipites regio
Baculapollenites grimsdaloide
Bacumonocolpites sp.
Echimonocolpites sp.
Gemmamonocolpites (all species)
Gemmastephanocolpites (all species)
Mauritiidites (all species)
Monocolpopollenites (all species)
Monosulcites
Psilamonocolpites (all species)
Racemonocolpites (all species)

Spinizonocolpites (all species)
Trichotomosulcites (all species)

Olacaceae
Anacolosidites cf. *luteoides*

Bombacoideae
Bombacacidites (all species)
Retistephanocolporites minimus (Bombacaceae type)

Onagraceae
Corsinipollenites

Fabaceae
Crassiectoapertites
Margocolporites
Polyadopollenites
Striatopollis catatumbus

Euphorbiaceae
Croton type
Crototricolpites pachidermatus
Crototricolpites sp.*1DO*
Ranunculacidites operculatus
Retitrescolpites? *irregularis*

Ctenolophonaceae
Ctenolophonidites lisamae
Verrustephanocolpites rugulatus

Proteaceae
Echitriporites trianguliformis
Echitriporites trianguliformis orbicularis
Proteacidites
Retidiporites magdalenensis

Araceae
Ephedripites chomotrileticus
Ephedripites rizadus
Proxapertites extrañus
Proxapertites heterofoveolatus
Proxapertites cursus
Proxapertites minutus
Proxapertites operculatus
Proxapertites psilatus
Proxapertites sp.

Proxapertites verrucatus
Proxapertites imperialis
Proxapertites inmensus
Proxapertites nexinatus
Spathiphyllum sp. 1_PETM
Spathiphyllum vanegensis

Annonaceae
Proxapertites aff. *tertiaria*
Proxapertites magnus
Proxapertites humbertoides
Proxapertites tertiaria
Proxapertites minutihumbertoides
Proxapertites heterofoveolatus
L. proxapertitoides proxapertitoides
L. proxapertitoides reticuloides
Longapertites (all species)

Ericaceae
Ericipites aff. *annulatus*

Moraceae
Momipites (all species)
Psiladiporites (all species)

Poaceae
Monoporopollenites (all species)

Polypodiaceae
Polypodiisporites

Convolvulaceae
Perfotricolpites (all species)

Rhizophoraceae
Paleosantalaceaepites (all species)
Zonocostites (all species)

Podocarpaceae
Podocarpidites

Sterculioideae
Rhoipites miniguianensis
Rhoipites guianensis

Sapotaceae

Tetracolporopollenites (all species)

Ulmaceae
Ulmoideipites krempii

Myrtaceae
Syncolporites poricostatus

Pelliceriaceae
Lanagiopollis (all species)

Passifloraceae
Spirosyncolpites spiralis

5.9 Aridity vs Rainfall Analysis

Plant families identified in this study were classified as wet or dry, according to the analysis of Punyasena (S79), that identified Family precipitation preferences based on the Gentry's 144-transect neotropical plant database (Table S9). Fabaceae are both abundant in high rainfall and dry habitats within the tropics (S80). However, to be more conservative, Fabaceae was considered to be an indicator of dryness. Then, the sum of abundances of the families corresponding to each category (wet versus dry) was calculated for each sample of the Mar2x core (only samples with sums larger than 80 grains were used). The results (Table S9) indicate that both Paleocene and Eocene samples are dominated by families indicating wet habitats and there is not a significant difference in their combined relative abundances across the Paleocene-Eocene (Paleocene= 64%, Eocene= 61%, t-test, $p < 0.49$, df: 32.5). Abundance of dry elements (e.g., grasses) represents <2% of the assemblage (Paleocene=0.7%, Eocene=2%).

5.10 Rates of Origination and Extinction

Per capita rates of origination and extinction were calculated following Foote (S62) using the package *Stratigraph.* The bin used was the stratigraphic thickness of the PETM in the Mar 2x site (which was assumed to have accumulated for 200,000 years, the upper estimate of the duration of the PETM (S81), in order to be able to compare the PETM interval with levels below and above. These rates were not calculated in either

Riecito Mache or Gonzales, because the analyzed stratigraphic interval was not long enough.

6. Temperature Analysis

6.1 Estimation of Temperature

We estimate the mean annual temperature (MAT) of the region during the Late Paleocene, using both published information and data measured in this study (TEX_{86} from P2 core, a nearby marine site, 300 km west of Mar2x, that is described in subsequent headings 6.1 and 6.2). Sea-surface temperature (SST) from Tanzania was ~29 °C at the uppermost Paleocene (S82). Published temperatures for Cerrejon, a Late Paleocene terrestrial site that is 50 km west of Mar2x, ranges from 28 to 34 °C (S15,S83,S84). Using a snake paleothermometer, Head et al (S79, S80) produced two estimates of MAT, first 30-34 °C (S83), and later a refined estimation of 28-31 °C (S84). Here, we use the cooler estimate (28-31 °C) that seems to be in agreement with other proxies.

Our own estimates for the Late Paleocene, derived from TEX_{86} of core P2, yielded TEX_{86} values that were relatively low in the Late Paleocene (0.65-0.73, Table S10). To estimate SST from TEX_{86}, two calibrations (S85,S86) were applied that yielded similar estimates with an average of 28.2 ± 1.4 °C (S85) and 27.3 ± 1.1 °C (S86) for this time period. In summary, considering all proxies together, the range of MAT for the late Paleocene in the region was likely 28-31 °C.

We estimated the increase in MAT during the PETM, using both published data and also TEX_{86} data from P2 core. Zachos et al. (S87) found an increase of 3-5 °C during the PETM in tropical Pacific sea-surface temperature (SST), slighty lower than estimates from high and mid latitude sites (S88,S89). We do not have a direct estimation of the temperature of the PETM in any of our sites, as they did not contain suitables sediments. Instead, we used the SST of the Early Eocene that was determined in core P2, as a proxy for the MAT during the PETM, because the absolute temperature increase was similar in both the Early Eocene and the PETM. Early Eocene TEX_{86} values were higher than the Paleocene (0.75-0.87, Table S10). SST estimates are 31.5 ± 2.3 °C (S85) and 29.7 ± -1.6 °C (S86), or a ~2-4 °C increase relative to late Paleocene values. This increase in SST calculated by TEX_{86} is in agreement with the 3-5 °C calculated by Zachos et al. (S87). Therefore, a conservative estimate of the increase in MAT during the PETM could be in the order of 3°C assuming a similar increase in MAT compared to SST. If the MAT of the Late Paleocene was 28-31 °C, then the MAT during the PETM was likely ~31-34 °C.

6.2 TEX_{86} analysis

Samples from a sediment core from Northeastern Colombia (P2, 9.541679° N, 75.337792° W, paleolatitude= 7.06° N, 77.1° W, paleolatitude calculated using GPlates (S90)), were analyzed for TEX_{86} (Table S10). Organic compounds were extracted from powdered and freeze- dried sediments with dichloromethane (DCM)/ methanol (MeOH) (9:1, v/v) by using the accelerated solvent extraction technique (Dionex). Excess solvent was removed using a rotary evaporation with vacuum. The total extracts were separated in polar and apolar fractions over an activated Al_2O_3 column using hexane:DCM (1:1, v/v) and DCM:MeOH (1:1, v/v), respectively. The polar fraction was then dissolved in a 99:1 (v/v) hexane/isopropanol mixture, and sieved using a 0.45 µm, 4 mm diameter polytetrafluoroethylene (PTFE) filter, before being analyzed using a high-performance liquid chromatography/atmospheric pressure positive ion chemical ionization mass spectrometer (HPLC/ APCI-MS). HPLC/APCI-MS analyses were done according to Schouten et al. (S91) using an Agilent 1100 series LC/MSD SL and separation and a Prevail Cyano column (2.1 × 150 mm, 3 mm; Alltech), maintained at 30 °C. The GDGTs were eluted using a changing mixture of hexane and isopropanol as follows: 99% hexane to 1% propanol for 5 minutes, then a linear gradient to 1.8% isopropanol for 45 minutes. Flow rate was 0.2 ml per minute. Single ion monitoring was set to scan the 5 $[M+H]+$ ions of the GDGTs with a dwell time of 237 ms for each ion. GDGT signals were generally low, especially at the lower levels where intense weathering was observed, suggesting that GDGTs were degraded in these sections. The values reported here were those where all GDGT isomers used in the TEX_{86} were above the limit of quantification (S92). This threshold resulted in the rejection of about two-thirds of the data of all sediments analyzed. We applied the core top calibration equations of Kim et al.(S85):

$$T = 38.6 + 68.4 \text{ x } \log (TEX_{86})$$

and that of Liu et al. (S86):

$$T = -16.33 \times 1/TEX_{86} + 50.475$$

In order to translate TEX_{86} values into an estimate of mean annual sea-surface temperature. The calibrations give roughly similar SST estimates for the late Paleocene but the Liu et al. (S86) calibration gives lower early Eocene estimates because it is non-linear toward higher temperatures. BIT values, a proxy for the input of soil organic matter, were below 0.2 in all cases, suggesting that the TEX_{86} values were not affected by a contribution of soil-derived tetraether lipids.

6.3 Core P2, NE Colombia

6.3.1 Description Core P2, NE Colombia

Core P2 (9.541679° N, 75.337792° W) was drilled in the northeastern region of Colombia in the Sinu-San Jacinto. During the Paleocene–Eocene transition, the northeastern part of South America was under dextral transpression, with oblique subduction of the Caribbean Plate under continental crust of northern Colombia (S93). Modern paleoenvironmental models (S94) indicate the presence of a shallow platform and deltaic systems in the Colombian Caribbean region (Sinu-San Jacinto Fold Belt). Core P2 (Fig. S14) has massive dark-gray to black calcareous mudstones, rich in organic matter rich, occasionally with horizontal bioturbation or plane-parallel beds; this lithology has intercalation of fining-upward sequences of calcareous litarenites, generally massive, with horizontal bioturbation and wavy lamination, and flaser and hummocky structure. Sediments suggest deposition in a prodeltaic environment. There are no major lithological changes across the Paleocene–Eocene transition.

6.3.2 Biostratigraphic Dating Core P2, NE Colombia

The age of the core was determined by using the planktonic foraminiferal zonation of Berggren (Fig S14) (S45,S95). Pollen recovery in the core was scarce, but confirms the age given by foraminifera. The late Paleocene was recognized by planktonic foraminifera zones P3 and P4. Zone P3 (from the first appearance of *Morozovella angulata* and/or *Igorina pusilla* to the first appearance of *Globanomalina pseudomenardii*) is represented by an interval dominated by *Morozovella aequa, M. subbotinae* and *Subbotina variospira*. Nine samples from the 189.36-134.26 m interval contain the P3 assemblage. However, this zone cannot be sharply defined. According to various sources (S45,S46,S95), Zones P3 and P4 are distinguished by the first appearance of *Morozovella angulata* and/or *Igorina pusilla* and the first appearance of *Globanomalina pseudomenardii*. In the core, *M. angulata* occurs only in two samples from the upper part of Zone P4; *I. pusilla* was not recognized. The first appearance of *Globanomalina pseudomenardii* is at 211.13m. Other species *Morozovella aequa* and *M. acuta* usually occurs slightly above the base of Zone P3. The benthic assemblage is dominated by *Spiroplectammina grzybowskii* and *Rzehakina epigona.* Zone P4 is defined as the total range of *Globanomalina pseudomenardii* (S45,S46,S95). *G. pseudomenardii* occurs in the interval from 211.13 to 309.62 m, whereas definite Zone P5 starts at 316.62 m, as discussed below. The absence of *G. pseudomenardii* in the 316.62–334m interval may be due either to poor preservation of planktonic foraminifers or to extinction of the taxon. The Zone P4 marker (*Globanomalina pseudomenardii*) is last observed at 309.62 m and the last appearance of *Morozovella acuta* is at 316.62 m. The last appearances of *Morozovella aequa* and *Globanomaina chapmani* are at 334 m. Four samples were studied between these last two levels. Among them, one (at 319.88m) has no planktonic foraminifers and calcareous nannofossils are also absent, and a stratigraphic designation is difficult. The sample at 316.62 m contains neither *G. pseudomenardii* nor *Morozovella subbotinae.* Because the P4/P5 zone boundary is primarily defined by either the last appearance of *G. pseudomenardii* or the first appearance of *Morozovella subbotinae*, the sample should belong to Zone P5. However, the biostratigraphic zonation of the 325.66–334 m interval is represented by a condensed interval treated as belonging to Zone P6, because it does not contain *M. acuta.* Because of poor preservation, the diversity of planktonic foraminiferal assemblages in Zone P5 is lower than in Zones P4 and P6. The early Eocene was recognized by zone P6. Species occurring in Zone P5 are common open-marine taxa. The original diversity may have been higher, because dissolution may have removed some fragile shells and recrystallization also makes recognition of some zones difficult. As stated above, Zone P6 cannot be unequivocally separated from Zone P5 on the basis of planktonic foraminiferal and nannofossils biostratigraphy alone because of the rare occurrence of micro and nannofossils between 316.88 and 334 m. As a result of rare occurrence secondary datum events to mark the definite top, Zone P5 includes the last appearance of *Morozovella acuta* and Zone P6 includes the last appearance of *Morozovella aequa* and *Globanomalina chapmani.* In addition, the calcareous nannofossils *Chiasmolithus bidens, Fascicuithus tympaniformis* and *Neochiastozygus saepes* occur in the base of nannofossil Zone NP10, at 325.66 m. Planktonic foraminiferal biostratigraphy places the base of Zone P6 and the base of the Eocene above the last appearance of *Morozovella acuta* at 316.62 m, as discussed above. Nannofossil biostratigraphy indicates an early Eocene age at 325.66 m.

Supplementary References

S1. R-Development-Core-Team. (R Foundation for Statistical Computing, Vienna, Austria, 2009).
S2. W. Green, C. Jaramillo, F. de-la-Parra. (2010).
S3. J. Oksanen *et al.* (R for Statistical Computing, 2010).
S4. M. Maechler, P. Rousseeuw, A. Struyf, M. Hubert. (2005).
S5. O. A. Colmenares, L. Terán, Palynology 17, 67 (1993).
S6. A. Fabre, Geología Norandina 4, 3 (1981).
S7. C. Caceres, F. Cediel, F. Etayo, Maps of Sedimentary Facies Distribution and Tectonic Setting of Colombia through the Proterozoic and Phanerozoic. (Ingeominas, Bogota, ed. 1, 2005), pp. 42.
S8. H. Caceres, R. Camacho, J. Reyes, in Geological Field-Trips, Colombia 1980-1989. (Asociación Colombiana de Geólogos y Geofísicos del Petróleo, Bogotá, 1980), pp. 1-31.
S9. A. E. Gonzalez, A palynologic study on the upper Los Cuervos and Mirador formations (lower and middle Eocene), Tibú Area, Colombia. (E.J. Brill, Leiden, 1967), pp. 68.
S10. O. A. Colmenares, L. Terán, Revista Técnica Intevep 10, 209 (1990).
S11. V. Rull, Review of Palaeobotany and Palynology 107, 83 (1999).
S12. B. Murat, M. Ruiz, "Estudio sedimentológico de las formaciones Marcelina y Guasare en los núcleos del Pozo MAR-2x, Distrito Mara, Estado Zulia" (MARAVEN, 1994).
S13. T. Westerhold *et al.*, Palaeogeography, Palaeoclimatology, Palaeoecology 257, 377 (2008).
S14. N. C. Arens, A. H. Jahren, R. Amundson, Paleobiology 26, 137 (2000).
S15. S. L. Wing, G. J. Harrington, F. Smith, J. I. Bloch, D. M. Boyer, Science 310, 993 (2005).
S16. T. Westerhold, U. Röhl, H. K. McKarren, J. C. Zachos, Earth and Planetary Science Letters 287, 412 (2009).
S17. J. A. Aspden, W. J. McCourt, M. Brook, Journal of the Geological Society 144, 893 (1987).
S18. E. G. Lidiak, W. T. Jolly, International Geology Review 38, 1098 (1996).
S19. U. Röhl, T. Westerhold, T. J. Bralower, J. C. Zachos, Geochemistry Geophysics Geosystems 8, Q12002 (Dec, 2007).
S20. U. Röhl, T. J. Bralower, R. D. Norris, G. Wefer, Geology 28, 927 (2000).
S21. S. J. A. Brown, R. T. Smith, Journal of Volcanology and Geothermal Research 135, 247 (2004).
S22. K. D. McCormacka, M. A. Mary-Gee, N. J. McNaughton, R. Smith, I. R. Fletcher, Journal of Volcanology and Geothermal Research 183, 97 (2009).
S23. K. R. Ludwig, Isoplot 3.00. Special Publication (Berkeley Geochronology Center Berkeley, 2003), vol. 4, pp. 70.
S24. A. H. Jaffey, K. F. Flynn, L. E. Glendenin, W. C. Bentley, A. M. Essling, Physical Reviews C 4, 1889 (1971).
S25. Z. Chang, J. D. Vervoort, W. C. Mcclelland, C. Knaack, Geochem Geophy Geosy 7, (2006).

S26. J. Kosler, P. Sylvester, Reviews in Mineralogy & Geochemistry 53, 243 (2003).
S27. S. M. Eggins, L. P. J. Kinsley, J. M. G. Shelly, Appl. Surf. Sci. 127, 278 (1998).
S28. W. R. Dickinson, G. E. Gehrels, Sedimentary Geology 163, 29 (2003).
S29. J. B. Paces, J. D. Miller, Journal of Geophysical Research 98, 13997 (1993).
S30. K. DeGraaff–Surpless, J. L. Wooden, M. O. McWilliams, Geological Society of America Bulletin 114, 1564 (2002).
S31. I. S. Williams, Reviews in Economic Geology 7, 1 (1998).
S32. J. M. Mattinson, Chemical Geology 220, 47 (2005).
S33. T. E. Krogh, Geochimica et Cosmochimica Acta 37, 485 (1973).
S34. H. Gerstenberger, G. Haase, Chemical Geology 136, 309 (1997).
S35. M. D. Schmitz, B. Schoene, Geochem. Geophys. Geosyst. 8, Q08006 (2007).
S36. J. L. Crowley, B. Schoene, S. A. Bowring, Geology 35, 1123 (2007).
S37. G. Bayona *et al.*, Geological Society of America Bulletin 120, 1171 (2008).
S38. J. H. Germeraad, C. A. Hopping, J. Muller, Review of Palaeobotany and Palynology 6, 189 (1968).
S39. C. Jaramillo *et al.*, in Geological Problem Solving with Microfossils: A Volume in Honor of Garry D. Jones, T. Demchuk, R. Waszczak, Eds. (SEPM Special Publication, Tulsa, 2009), vol. 93, pp. 29-40.
S40. C. A. Jaramillo, D. L. Dilcher, Palaeontographica B 258, 87 (2001).
S41. M. Lorente, Palynology and Palynofacies of the Upper Tertiary in Venezuela. (J. Cramer, Berlin, 1986), pp. 222.
S42. J. Muller, E. Di Giacomo, A. Van Erve, American Association of Stratigraphic Palynologists Contribution Series 19, 7 (1987).
S43. M. Regali, N. Uesugui, A. Santos, Boletim Tecnico da Petrobras 17, 177 (1974).
S44. C. Jaramillo, F. Muñoz, M. Cogollo, F. Parra, in Recent Developments in Applied Biostratigraphy, A. J. Powell, J. Riding, Eds. (The Micropaleontological Society Special Publications, London, 2005), pp. 145-159.
S45. W. A. Berggren, D. V. Kent, C. C. Swisher II, M. Aubry, in Geochronology time scales and global stratigraphic correlation, W. A. Berggren, D. V. Kent, M. P. Aubry, J. Hardenbol, Eds. (SEPM, Tulsa, 1995), vol. 54, pp. 129-212.
S46. F. M. Gradstein, J. G. Ogg, A. Smith, A Geologic Time Scale 2004. (Cambridge University Press, New York, 2005), pp. 610.
S47. T. Van der Hammen, Boletín Geológico (Bogotá) 2, 49 (1954).
S48. T. Van der Hammen, Boletín Geológico (Bogotá) 5, 49 (1957).
S49. T. Van der Hammen, C. García, Leidse Geologische Mededelingen 35, 105 (1966).
S50. H. Carvajal-Ortiz, G. Mora, C. Jaramillo, Palaeogeography, Palaeoclimatology, Palaeoecology 277, 173 (2009).
S51. C. Jaramillo, M. Rueda, G. Mora, Science 311, 1893 (2006).
S52. J. Zachos, M. Pagani, L. Sloan, E. Thomas, K. Billups, Science 292, 686 (2001).
S53. C. Jaramillo *et al.*, Palynology 31, 153 (2007).
S54. H. J. B. Birks, J. M. Line, The Holocene 2, 1 (1992).
S55. G. Harrington, Evolutionary Ecology Research 6, 33 (2004).
S56. J. Haskell, Evolutionary Ecology Research 3, 345 (2001).
S57. C. A. Jaramillo, Paleobiology 28, 222 (2002).

S58. R. J. Morley, Origin and evolution of tropical rain forests. (John Wiley & Sons, New York, 2000), pp. 362.
S59. B. V. Odgaard, Journal of Biogeography 26, 7 (1999).
S60. B. V. Odgaard, Diversity and Distributions 7, (2001).
S61. A. Traverse, Paleopalynology, Second Edition. (Springer, Dordrecht, 2007), pp. 813.
S62. M. Foote, in Deep time: Paleobiology's perspective, D. H. Erwin, S. L. Wing, Eds. (The Paleontological Society, Lawrence, 2000), vol. 26, pp. 74-102.
S63. SPSS, Systat 9, statistics II. (SPSS Inc., Chicago, 1999), pp. 552.
S64. D. P. Yeager, G. R. Ultsch, Physiological Zoology 62, 888 (1989).
S65. R. G. Duggleby, L. C. Ward, Physiological Zoology 64, 885 (1991).
S66. W. L. Kovach, Review of Palaeobotany and Palynology 60, 255 (1989).
S67. L. Kaufman, P. J. Rousseeuw, Finding Groups in Data. (John Wiley & Sons, New Jersey, 2005), pp. 342.
S68. D. M. Raup, Paleobiology 1, 333 (1975).
S69. A. E. Magurran, Measuring Biological Diversity. (Blackwell Publishing, Malden, Massachusetts, 2004), pp. 256.
S70. R. J. Burnham, A. Graham, Annals of the Missouri Botanical Garden 86, 546 (1999).
S71. R. J. Burnham, K. R. Johnson, Philosophical Transactions of the Royal Society of London Series B Biological Sciences 359, 1595 (2004).
S72. C. Hoorn, Palaeogeography, Palaeoclimatology, Palaeoecology 112, 187 (1994).
S73. C. Jaramillo *et al.*, in Amazonia, Landscape and Species Evolution, M. C. Hoorn, F. P. Wesselingh, Eds. (Blackwell, Oxford, 2010), pp. 317-334.
S74. C. Jaramillo, M. Rueda. (Colombian Petroleum Institute & Smithsonian Tropical Research Institute, 2010).
S75. T. Van der Hammen, Boletín Geológico (Bogotá) 6, 67 (1958).
S76. T. Van der Hammen, T. A. Wymstra, Leidse Geologische Mededelingen 30, 183 (1964).
S77. W. A. Van der Kaars, Geología Norandina 8, 33 (1983).
S78. T. A. Wijmstra, The Palynology of the Guiana Coastal Basin. (Drukkerij de Kempenaer, Oegstgeest, Utrecht, 1971), pp. 62.
S79. S. W. Punyasena, G. Eshel, J. C. McElwain, Journal of Biogeography 35, 117 (2008).
S80. S. W. Punyasena, Palaeogeography, Palaeoclimatology, Palaeoecology 265, 226 (2008).
S81. U. Röhl, L. J. Abrams, Proceedings of the Ocean Drilling Program, Scientific Results 165, 191 (2000).
S82. P. N. Pearson *et al.*, Geology 35, 211 (2007).
S83. J. Head *et al.*, Nature 457, 715 (2009).
S84. J. Head *et al.*, Nature 460, E4 (2009).
S85. J.-H. Kim *et al.*, Geochimica et Cosmochimica Acta 74, 4639 (2010).
S86. Z. Liu *et al.*, Science 323, 1187 (2009).
S87. J. C. Zachos *et al.*, Science 302, 1551 (2003).
S88. A. Sluijs *et al.*, Nature 441, (2006).
S89. J. C. Zachos *et al.*, Geology 34, 737 (2006).

S90. University_of_Sidney, Geological_Survey_of_Norway, California_Insitute_of_Technology. (2010).
S91. S. Schouten, C. Huguet, E. C. Hopmans, J. S. Sinninghe-Damsté, Anal. Chem. 79, 2940 (2007).
S92. S. Schouten, A. Forster, F. E. Panoto, J. S. Sinninghe-Damsté, Organic Geochemistry 38, 1537 (2007).
S93. L. Kennan, J. L. Pindell, Geological Society of London Special Publications 328, 487 (2009).
S94. Universidad_de_Caldas-ANH, “Estudio integrado de los núcleos y registros obtenidos de los pozos someros tipo “slim holes” en la Cuenca Sinú. ” (Internal report to ANH (Agencia Nacional de Hidrocarburos, Colombia), 2009).
S95. W. A. Berggren, P. N. Pearson, Journal of Foraminiferal Research 35, 279 (2005).

Supplementary Figures

Fig. S1. Lithological description of the Mar 2x Core, Maracaibo, Venezuela.

Fig. S2. Polygonal of the Riecito Mache section, Maracaibo, Venezuela.

Fig. S3. Lithological description of the Riecito Mache, Maracaibo, Venezuela.

Fig. S4. Polygonal of the Gonzales section, Catatumbo, Colombia.

Fig. S5. Lithological description of the Gonzales outcrop and Gonzales well, Catatumbo, Colombia.

Fig S6. Plot of the ^{206}Pb-^{238}U dates from the youngest zircon from the Riecito Mache tuff obtained by the U-Pb CA-TIMS method. Plotted with Isoplot 3.0 (S23). Error bars are 2σ internal errors. Weighted mean date is represented by the grey box behind the error bars. Error bars in white were not used in the weighted mean calculation.

Fig S7. U-Pb LA-ICP-MS TUFFZIRC age from the Riecito Mache tuff. Plotted with Isoplot 3.0(S23).

Fig. S8. Carbon isotope data (δ^{13}C) vs. Stratigraphic position, Mar 2x section following the method by (S15). A. Total organic carbon (TOC) vs. carbon isotope data (δ^{13}C). B. Residual of correlation TOC - δ^{13}C vs. the stratigraphic position. Pattern is very similar to raw δ^{13}C data.

Fig. S9. Carbon isotope data (δ^{13}C) vs. stratigraphic position, Riecito Mache section following the method by (S15). A. Total organic carbon (TOC) vs. carbon isotope data (δ^{13}C). B. Residual of correlation TOC - δ^{13}C vs. the stratigraphic position. Pattern is very similar to raw δ^{13}C data.

Fig. S10. Carbon isotope data ($\delta^{13}C$) vs. stratigraphic position, Gonzales section following the method by (S15). A. Total organic carbon (TOC) vs. carbon isotope data ($\delta^{13}C$). B. Residual of correlation TOC - $\delta^{13}C$ vs. the stratigraphic position. The pattern observed is very similar to that of the raw $\delta^{13}C$ data.

Fig. S11. Carbon isotope data of the C25, C27 and C29 *n*-alkane ($\delta^{13}C_{25,}$ $\delta^{13}C_{27,}$ $\delta^{13}C_{29}$) vs. stratigraphic position, Mar 2x section. The shift in isotopic compositions are very similar to bulk $\delta^{13}C$ data and $\delta^{13}C_{31}$.

Fig. S12. Deuterium data of *n*-alkane 25, 27, 29, and 31 vs. stratigraphic position, Mar 2x section. A the distinct negative shift can be observed at the onset of the PETM.

Fig. S13. Agglomerative Cluster Analysis for Mar 2x, Riecito Mache and Gonzales. Samples in red belong to PETM interval. Samples in Mar 2x and Gonzales are measured as a well. Samples in Riecito Mache are measured as an outcrop.

Fig. S14. Lithological description of Core P2, San Jacinto-Sinu Belt, northwestern Colombia.

Supplementary Tables

Table S1. Stable carbon isotope ($\delta^{13}C$) stratigraphy for all studied sections.

Table S2. Biostratigraphic range chart files for Mar 2x (depths are given from the ground-surface).

Table S3. Biostratigraphic range chart files for Riecito Mache (depths are given as measured as an outcrop; greater measure= younger rock).

Table S4. Biostratigraphic range chart files for Gonzales (depths are given from the ground-surface).

Table S5. Analytical data from the U-Pb CA-TIMS zircon analysis of the Riecito Mache Tuff.

Table S6. Analytical data from the U-Pb LA-ICP-MS and CA-TIMS zircon analysis of the Riecito Mache Tuff.

Table S7. Mar 2x carbon isotope composition (C) and deuterium compositions (D) of n-alkanes with 25, 27, 29, and 31 carbon atoms. CPI=Carbon Preference Index.

Table S8. Diversity summary results for Mar2x, Riecito Mache and Gonzales sites. N=number of pollen and spores counted per sample; S=number of species per sample; SD=Standing Diversity, after range-through method and excluding singletons, numbers in red indicate samples with edge-effect that were excluded from standing diversity analysis; SI=Simpson Index (it was not calculated for samples with counts <80).

Table S9. Relative abundances of dry vs wet indicator for Mar2x core. Precipitation preferences of families identified in this study are derived from Punyasena study (S79) of Gentry's 144-transect neotropical plant database.

Table S10. P2 core TEX_{86} values, BIT indices and SST estimates following the calibration of Kim et al. (S85) and Liu et al. (S86).

Figure S1. Lithological description of the Mar 2x Core, Maracaibo, Venezuela

Figure S2. Polygonal of the Riecito Mache section, Maracaibo, Venezuela.

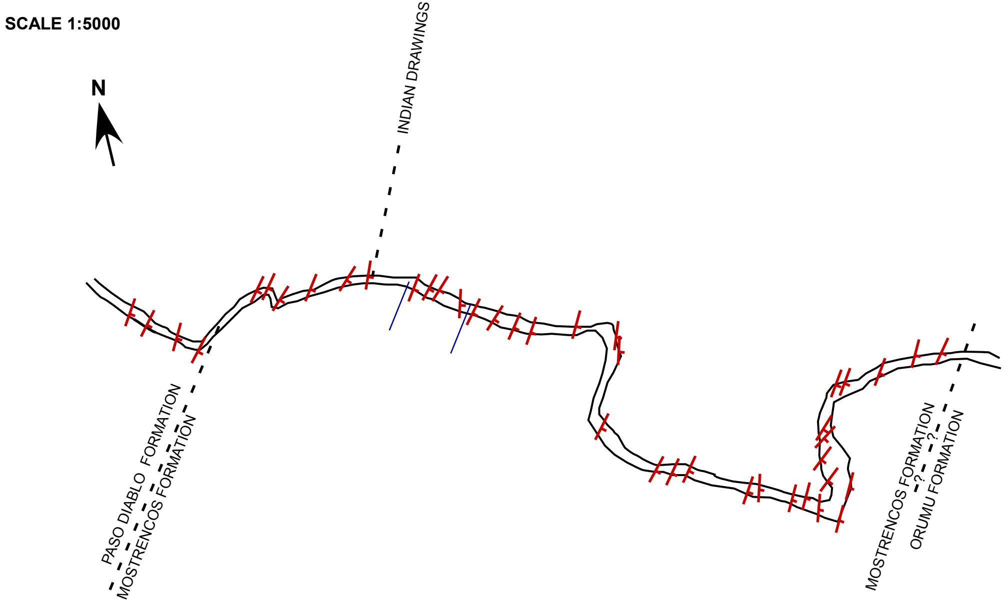

Figure S3. Lithological description of the Riecito Mache, Maracaibo, Venezuela.

Figure S4. Polygonal of the Gonzales section, Catatumbo, Colombia.

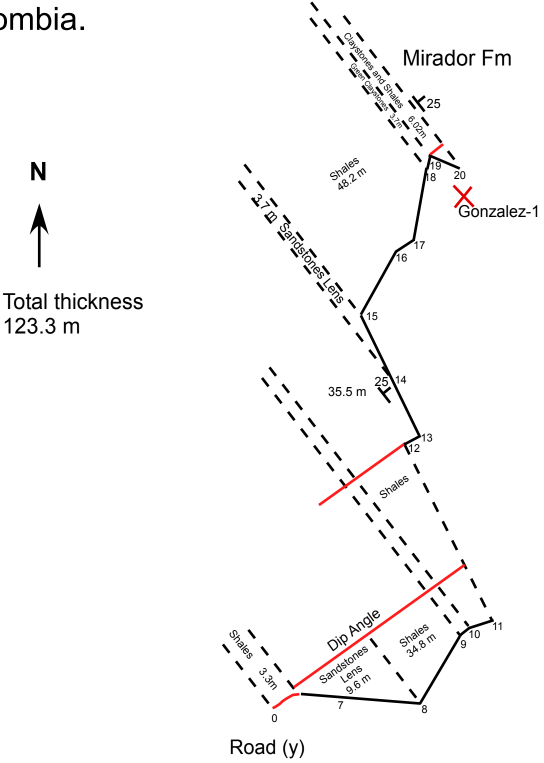

Figure S5. Lithological description of the Gonzales outcrop and Gonzales well, Catatumbo, Colombia.

Correlation Points

Gonzales	Outcrop(ft)	Gonzales Well (ft)
1	0.00	521.41
2	46.59	568.00
3	225.00	730.00
4	490.00	1130.00
5	500.10	1145.00

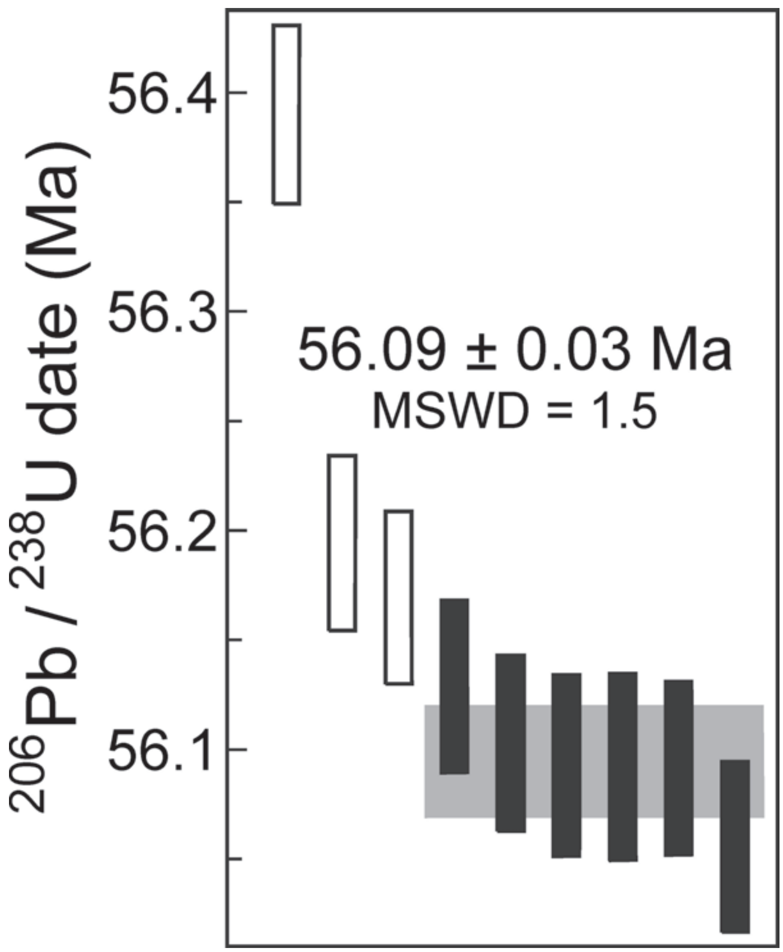

Fig. S6. Plot of the ^{206}Pb-^{238}U dates from the youngest zircon from the Riecito Mache tuff obtained by the U-Pb CA-TIMS method. Plotted with Isoplot 3.0 (S23). Error bars are 2σ internal errors. Weighted mean date is represented by the grey box behind the error bars. Error bars in white were not used in the weighted mean calculation.

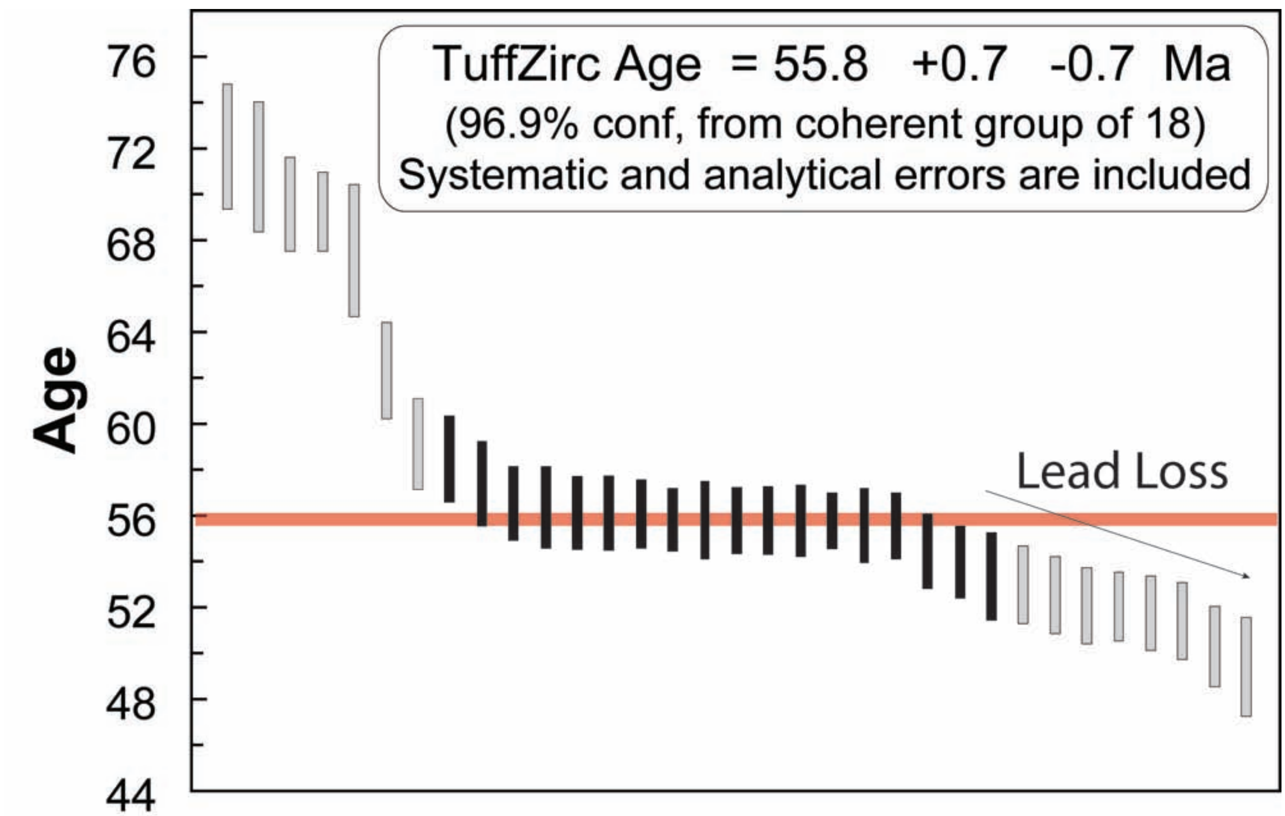

Fig. S7. U-Pb LA-ICP-MS TUFFZIRC age from the Riecito Mache tuff. Plotted with Isoplot 3.0 (S23).

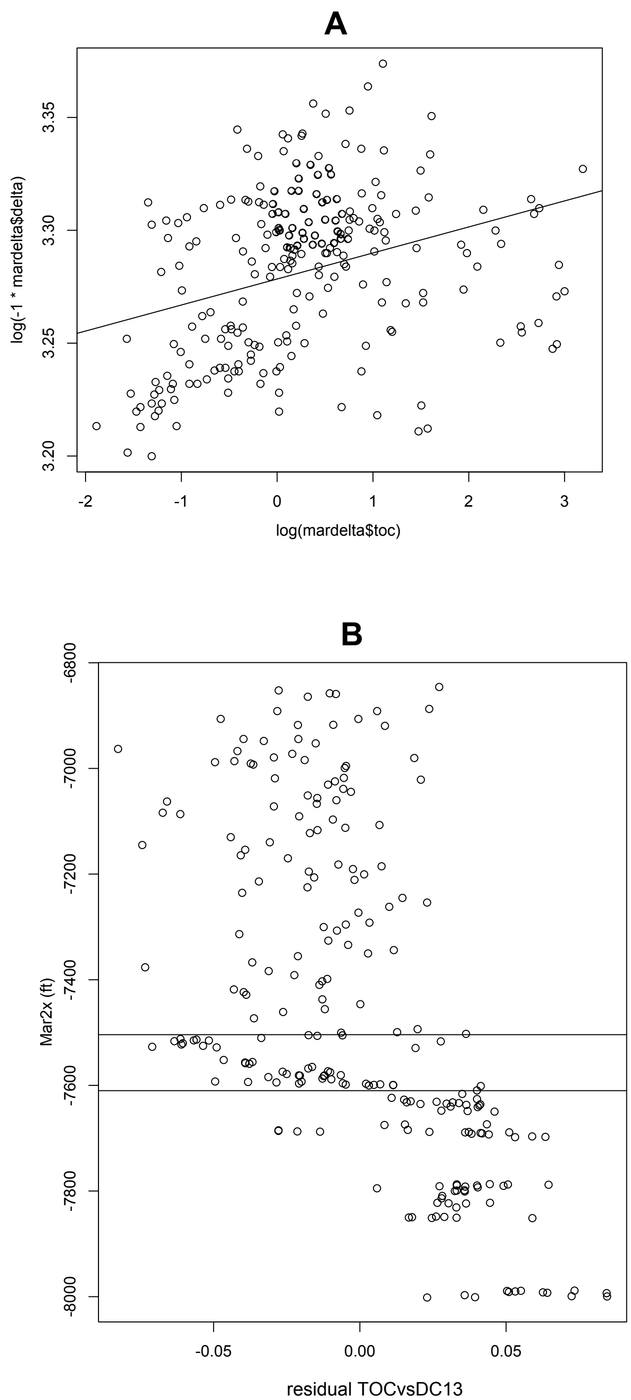

Fig. S8 Carbon isotope data ($\delta^{13}C$) vs. Stratigraphic position, Mar 2x section following the method by Wing et al (S*15)*. A. Total organic carbon (TOC) vs. carbon isotope data ($\delta^{13}C$). B. Residual of correlation TOC - $\delta^{13}C$ vs. the stratigraphic position. Pattern is very similar to raw $\delta^{13}C$ data.

A

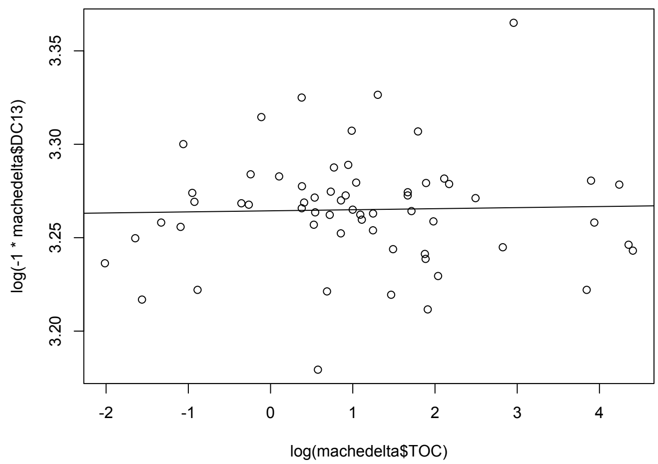

B

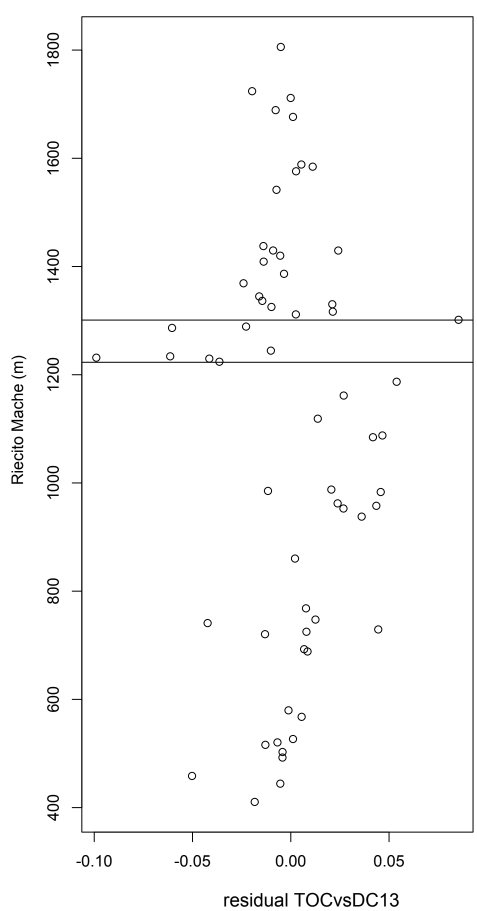

Fig. S9. Carbon isotope data (δ^{13}C) vs. stratigraphic position, Riecito Mache section following the method by Wing et al (*S15)*. A. Total organic carbon (TOC) vs. carbon isotope data (δ^{13}C). B. Residual of correlation TOC - δ^{13}C vs. the stratigraphic position. Pattern is very similar to raw δ^{13}C data.

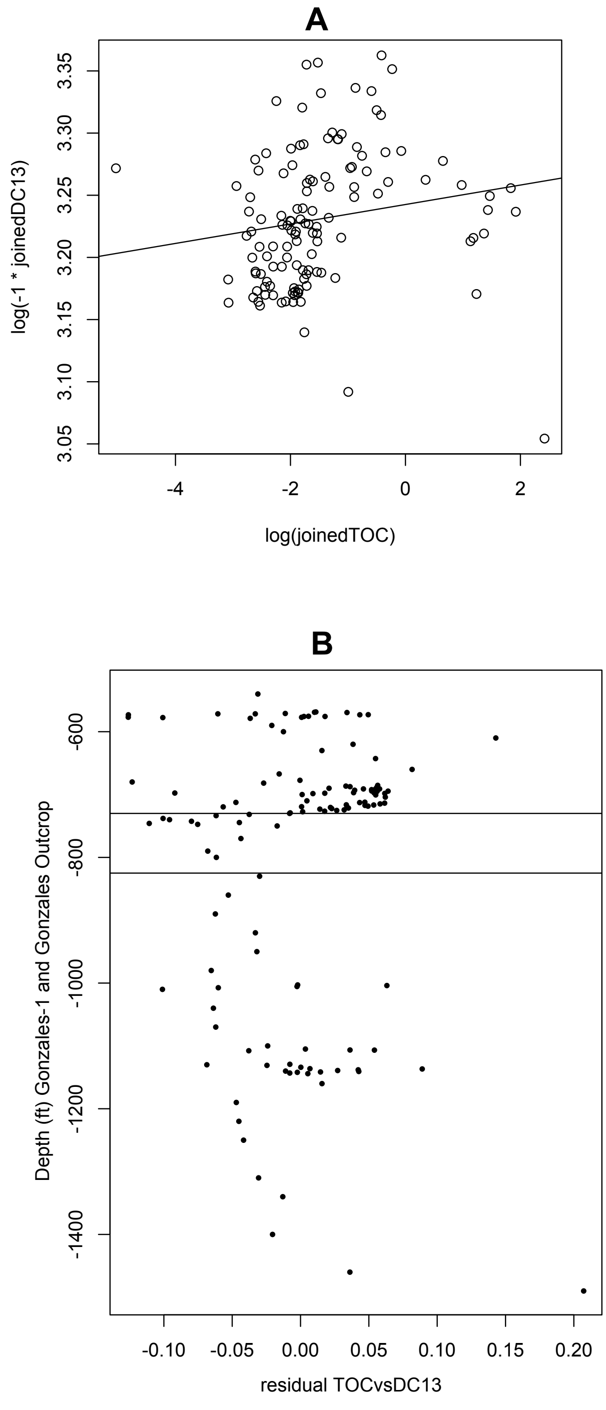

Fig. S10. Carbon isotope data ($\delta^{13}C$) vs. stratigraphic position, Gonzales section following the method by Wing et al (S*15)*. A. Total organic carbon (TOC) vs. carbon isotope data ($\delta^{13}C$). B. Residual of correlation TOC - $\delta^{13}C$ vs. the stratigraphic position. The pattern observed is very similar to that of the raw $\delta^{13}C$ data.

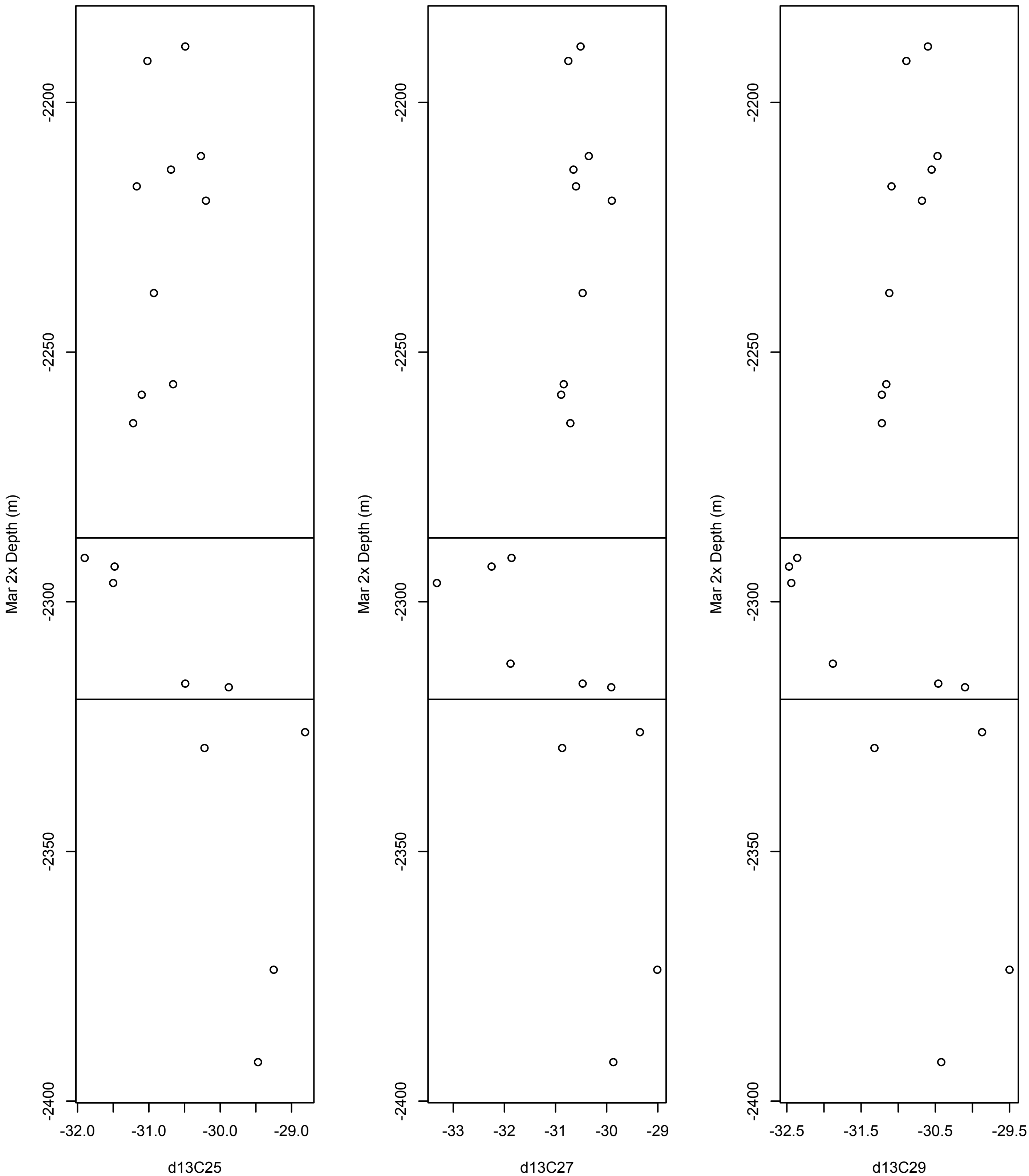

Fig. S11. Carbon isotope data of the C27, C27, and C29 *n*-alkanes ($\delta^{13}C_{25}$, $\delta^{13}C_{27}$, $\delta^{13}C_{29}$) vs. stratigraphic position, Mar 2x section. The shift in isotopic compositions are very similar to bulk $\delta^{13}C$ data and $\delta^{13}C_{31}$.

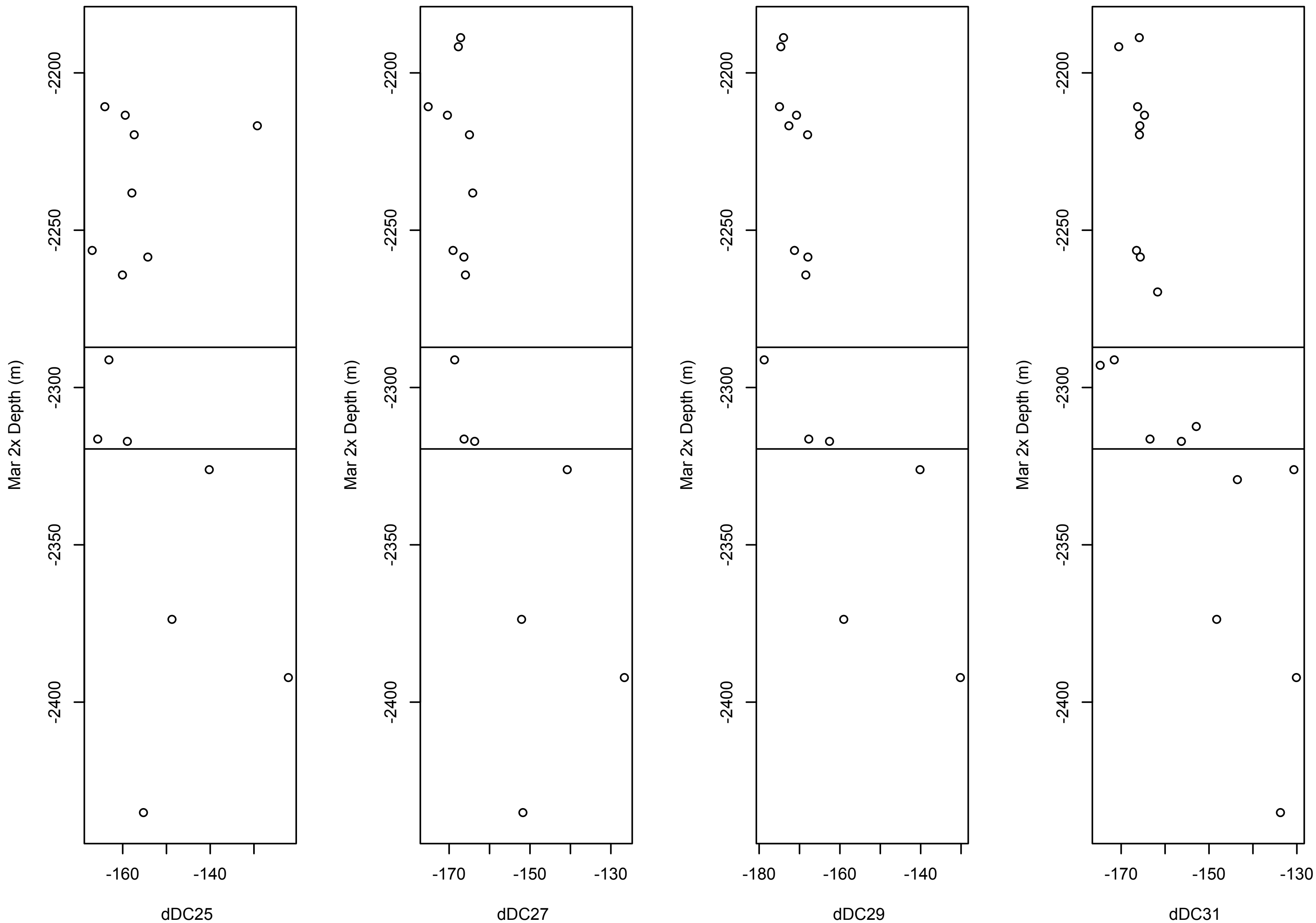

Fig. S12. Deuterium data of n-alkane 25, 27, 29 and 31 vs Stratigraphic position, Mar2x section. A distinct negative shift can be observed at the onset of the PETM.

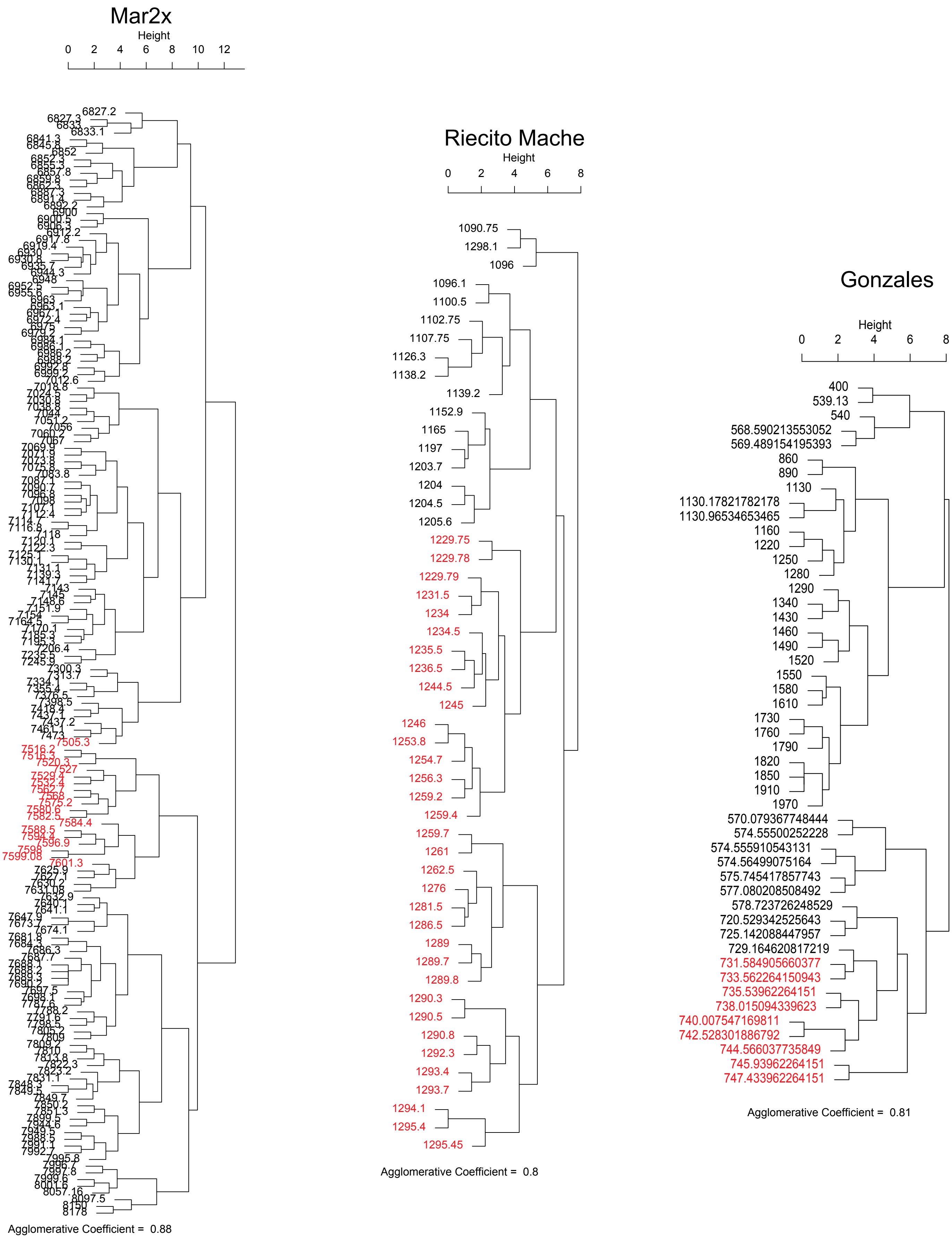

Figure S13. Agglomerative Cluster Analysis for Mar2x, Riecito Mache and Gonzales. Samples in red belong to PETM interval. Samples in Mar2x and Gonzales are measured as a well. Samples in Riecito Mache are measured as an outcrop.

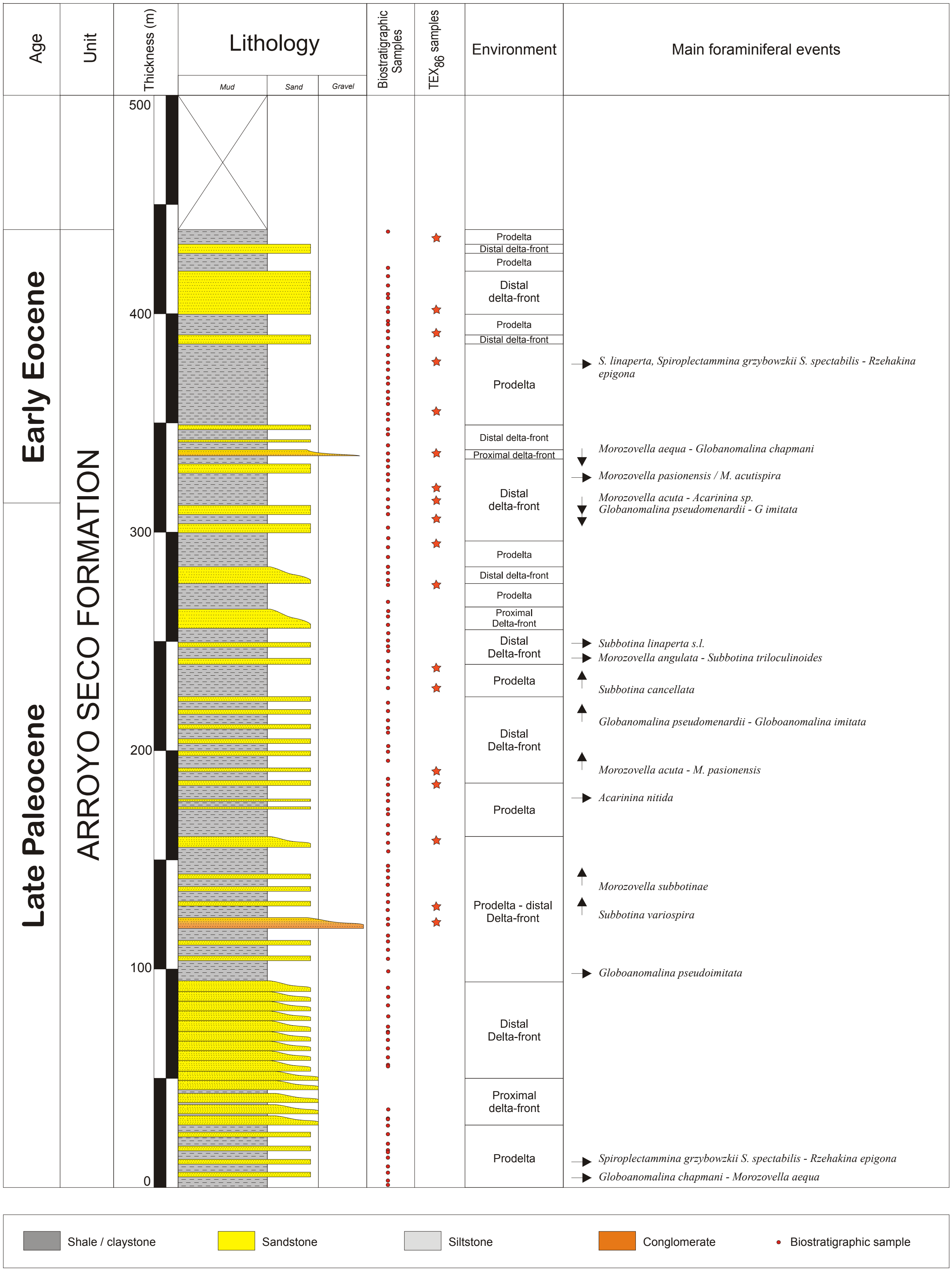

Figure S14. Lithological description of the P2 Core, San Jacinto-Sinu Belt, northwestern Colombia, including key biostratigraphic events, depositional environments and the stratigraphic position of the samples analyzed for biostratigraphy and TEX_{86}

Table S1. Stable carbon isotope stratigraphy for all studied sections.

MAR2x

depth (ft)	depth (m)	DC13	TOC
6944.3	2116.6	-27.31	1.9662
6845.8	2086.6	-26.41	6.9965
6852.3	2088.6	-27.56	2.4186
6859.1	2090.7	-26.83	1.2873
6864.3	2092.2	-27.26	2.2205
6887.3333	2099.3	-25.76	0.6003
6891.4	2100.5	-26.56	1.8172
6891.4167	2100.5	-27.49	1.8627
6906.25	2105	-28.11	2.4065
6906.3	2105	-26.86	2.7573
6917.4	2108.4	-26.96	1.8102
6917.75	2108.5	-27.34	2.1359
6919.4167	2109	-26.37	1.2286
6944.25	2116.6	-27.79	1.754
6948	2117.8	-27.55	1.5081
6952.5	2119.1	-26.9	0.8861
6963.0833	2122.3	-29.19	3.016
6967.0833	2123.6	-27.74	1.2525
6972.4167	2125.2	-27.02	0.6505
6979.1667	2127.3	-27.31	0.9525
6980.3	2127.6	-26.68	8.0803
6984.1	2128.8	-27.23	1.8389
6986.1667	2129.4	-27.87	1.7163
6988.1667	2130	-28.02	1.5393
6990.75	2130.8	-27.59	1.1616
6992.75	2131.4	-27.59	1.2517
6999.1667	2133.3	-26.72	1.1716
7017.9167	2139.1	-26.84	1.6819
7018.75	2139.3	-27.48	1.6819
7021.3	2140.1	-26.13	1.6123
7024.5	2141.1	-26.81	1.1725
7030.6667	2142.9	-26.88	1.1968
7038.75	2145.4	-26.84	1.6537
7044.3333	2147.1	-26.65	1.1209
7051.1667	2149.2	-27.05	1.1339
7056	2150.7	-27.01	1.3225
7060.1667	2151.9	-26.77	1.0761
7062.6667	2152.7	-28.59	2.128
7067	2154	-27.05	1.4827
7071.9167	2155.5	-27.33	1.0152
7083.8333	2159.2	-28.55	1.6599
7086.5	2160	-28.3	1.3024
7090.6667	2161.2	-27.14	1.1724
7684.33	2342.2	-25.78	0.34
7685	2342.4	-27.37	1.32
7686.25	2342.8	-27.31	1.09
7687.17	2343	-27.21	1.39
7687.67	2343.2	-27.35	4.25
7688.08	2343.3	-26.37	4.59
7688.17	2343.4	-25.92	3.32
7688.92	2343.6	-25.47	2.41
7689	2343.6	-25.38	0.48
7690.17	2344	-25.11	0.3
7690.92	2344.2	-25.02	0.23
7691.58	2344.4	-25.39	0.6
7692.92	2344.8	-25.03	0.29
7696.67	2345.9	-24.57	0.21
7697.5	2346.2	-24.53	0.27
7698.08	2346.4	-24.86	0.35
7787	2373.5	-25.33	0.84
7787.58	2373.7	-25.23	1.02
7788.17	2373.8	-25.07	1.96
7789.58	2374.3	-25.11	0.27
7790.25	2374.5	-24.85	0.24
7790.92	2374.7	-25.55	0.4
7791.58	2374.9	-25.27	0.33
7793.08	2375.3	-25.07	0.24
7798.5	2377	-25.47	0.64
7800	2377.4	-25.51	0.55
7800.92	2377.7	-25.33	0.4
7809.25	2380.3	-25.8	1.01
7813.75	2381.6	-26.26	4.59
7822.33	2384.2	-25.77	0.79
7823.17	2384.5	-25.66	0.76
7823.58	2384.6	-25.47	0.67
7831.08	2386.9	-25.48	0.52
7848.33	2392.2	-25.88	1.1
7849	2392.4	-25.81	1.11
7850.17	2392.7	-25.95	0.6202
7850.58	2392.9	-25.59	0.76
7851.33	2393.1	-25.02	1.02
7988.5	2434.9	-25.09	4.5033
7988.9	2435	-25.8	10.2694
7989.2	2435.1	-25.98	12.7155
7990.1	2435.4	-25.91	12.8548
7991.1	2435.7	-26.02	15.3048
7991.8	2435.9	-25.78	18.5313
7992.7	2436.2	-25.73	17.7254
7993.3	2436.4	-24.83	4.8116
7997.1	2437.5	-25.64	1.1606
7999.1	2438.1	-24.98	2.8423
7999.6	2438.3	-24.8	4.3749
8001	2438.7	-25.52	1.0298
8001.6	2438.9	-25.99	1.2185
6857.8	2090.3	-26.95	1.59265
6995.3	2132.2	-26.85	1.86725
7096.8	2163.1	-27.01	2.09234
7107.1	2166.2	-26.15	0.49878
7112.4	2167.9	-26.68	1.03135
7116.8	2169.2	-27.31	3.46007
7122.4	2170.9	-26.62	0.29807
7130.1	2173.3	-28.09	3.04727
7139.8	2176.2	-27.84	4.46899
7145	2177.8	-28.9	2.57958
7154	2180.5	-27.59	0.97215
7164.5	2183.7	-27.48	0.61828
7170.1	2185.4	-27.54	2.96232
7185.3	2190.1	-26.1	0.45761
7195.3	2193.1	-27.08	1.30279
7206.4	2196.5	-27.22	2.35227
7214	2198.8	-27.42	0.86927
7225.1	2202.2	-27.51	4.86425
7235.5	2205.4	-27.38	0.46507
7245.1	2208.3	-26.5	3.13205
7300.3	2225.1	-26.93	1.23465
7313.7	2229.2	-27.79	1.5292
7334.1	2235.4	-26.99	3.10714
7355.4	2241.9	-27.11	1.02914
7376.5	2248.4	-28.68	1.4566
7398.5	2255.1	-27.13	2.62498
7418.4	2261.1	-27.65	0.83832
7437.1	2266.8	-26.91	1.10973
7461.1	2274.1	-27.19	0.84709
7473	2277.8	-27.45	0.82779
7505.3	2287.6	-26.68	0.94705
7520.3	2292.2	-28.27	1.29026
7516.3333	2291	-28.29	1.06
7575.1667	2308.9	-27.01	1.94
7502.5	2286.8	-25.94	3.27
7573.1667	2308.3	-26.94	1.45
7522.6667	2292.9	-28.24	1.12
7594.4167	2314.8	-27.45	1.6
7506.25	2287.9	-27.25	2.85
7588.5	2313	-27.11	2.76
7513.3333	2290.1	-28.08	1.07
7514.8333	2290.5	-28.02	0.82
7593.5833	2314.5	-27.27	0.39
7558	2303.7	-27.18	0.27
7504.9167	2287.5	-27.24	2.13
7500.25	2286.1	-26.4	0.37
7568	2306.7	-26.69	0.36
7574.1667	2308.6	-26.98	0.43
7565.0833	2305.8	-26.86	0.7
7578.5	2309.9	-26.92	0.4
7593	2314.3	-27.38	2.7
7587.1667	2312.6	-27.21	2.92
7512.25	2289.7	-28.11	0.73
7525.1667	2293.7	-28.52	5.01
7527	2294.2	-28.35	0.66
7592.6667	2314.2	-27.45	0.26
7581.0833	2310.7	-27.09	0.99
7559.0833	2304	-27.46	0.74
7584.25	2311.7	-27.02	0.32
7516.75	2291.1	-26.7	18.93
7499.25	2285.8	-26.47	2.45
7581.5833	2310.9	-27.24	1.65
7596	2315.3	-27.36	8.602
7635.9167	2327.4	-25.15	0.3418
7599.1667	2316.2	-26.95	10.3579
7600.25	2316.6	-26.9	4.2852
7632.0833	2326.3	-25.95	0.5817
7623.5833	2323.7	-25.98	0.4116
7627.0833	2324.7	-25.99	0.6155
7599.0833	2316.2	-27.11	9.7701
7633.5	2326.7	-25.33	0.3366
7635.25	2327.2	-25.69	0.3655
7673.6667	2338.9	-24.86	0.1517
7641.0833	2329	-25.76	2.5247
7649.6667	2331.6	-24.97	0.2792
7599.5833	2316.4	-26.84	7.2495
7674.0833	2339.1	-26.18	1.1876
7631.0833	2326	-26.25	3.8282
7636.9167	2327.7	-25.21	0.2775
7601.25	2316.9	-26.33	18.4596
7616.1667	2321.4	-25.26	0.292
7634.5833	2327	-25.42	0.3175
7609.5	2319.4	-26.39	20.0829
7596.9167	2315.5	-27.31	14.6154
7648.5833	2331.3	-25.33	0.4349
7632.25	2326.3	-25.79	1.3306
7598	2315.9	-26.94	6.8235
7529.25	2294.9	-25.91	0.6611
7596.5	2315.4	-27.06	0.9036
7598.5	2316	-27.49	14.1673
7555.75	2303	-27.2	0.3561
7582.5	2311.1	-27.07	1.9398
7528.0833	2294.6	-27.93	1.2222
7556.6667	2303.3	-27.23	0.3142
7581.1667	2310.7	-26.9	1.15
7640.0833	2328.7	-25.35	0.2811
7211	2197.9	-26.56	0.9288
7350.25	2240.4	-26.68	2.0514
7253.92	2211	-26.26	2.9845
7367.17	2245.5	-28.04	4.9382
7580.58	2310.6	-26.75	1.1483
7510.25	2289.1	-27.43	0.9575
7799.25	2377.2	-25.55	0.6671
7794.83	2375.9	-26.27	0.6985
7625.92	2324.4	-25.45	0.8659
7326	2233	-26.74	0.7677
7262	2213.5	-26.43	1.6998
7630.17	2325.7	-25.97	0.6989
7428.5	2264.2	-27.48	0.7186
7403	2256.4	-27.11	2.1101
7273	2216.8	-26.68	1.5432
7383.58	2250.5	-27.7	2.7936
7409.75	2258.5	-27.1	1.8775
7446.25	2269.6	-27.38	15.423
7200.5	2194.7	-26.71	2.0135
7307	2227.2	-27.09	3.0624
7851	2393	-25.8	0.7418
7551.92	2301.8	-27.91	1.4161
7181.92	2189	-26.9	1.7353
7849.5	2392.5	-25.84	0.4719
7493.58	2284	-25.84	0.5564
7675	2339.3	-25.84	0.2082
7343.92	2238.4	-26.33	1.4008
7295.58	2223.7	-26.59	0.7919
7515	2290.6	-28.17	2.0411
7423.5	2262.7	-27.42	0.5513
7291.92	2222.6	-26.58	1.5456
7455.75	2272.5	-27.86	24.3101
7787.33	2373.6	-25.51	0.5827
7190.5	2191.7	-26.81	1.9974
7789.5833	2374.3	-25.22	0.2169
7647.9167	2331.1	-25.75	0.831
7391.25	2252.9	-27.14	1.016
7638.0833	2328.1	-25.47	0.9924
7822.3333	2384.2	-25.23	0.5994

RIECITO MACHE

Sample II	depth (m	DC13	TOC
SS 1361	410.5	-26.65	1.1099
SS 1355	444.25	-26.29	0.3963
SS 1354	458.5	-27.51	0.894
SS 1349	492.5	-26.27	0.7013
SS 1348	502.75	-26.28	1.5042
SS 1347	516	-26.51	1.465
SS 1346	520.5	-26.35	1.7101
SS 1345	526.75	-26.142	1.7211
SS 1342	567.75	-26	0.2644
SS 1340	579.75	-26.2	1.4612
SS 2172	688.5	-26	51.291
SS 1331	692.75	-26.016	7.2465
SS 1328	720.5	-26.542	8.773
SS 1327	725	-25.94	0.3349
SS 2168	729.25	-25.08	46.751
SS 1324	741	-27.31	2.6828
SS 1322	747.5	-25.85	2.3506
SS 1319	768.25	-25.97	1.6924
SS 1313	860.25	-26.126	3.4788
SS 1306	937.75	-25.267	7.67
SS 1305	952.75	-25.499	6.589
SS 1304	957.75	-25.059	1.987
SS 2161	962.25	-25.612	81.981
SS 1301	983.25	-25.014	4.334
SS 2159	985.25	-26.533	69.472
SS 2158	987.75	-25.693	77.802
SS 1296	1084.5	-25.08	0.4116
SS 1295	1087.75	-24.95	0.2094
SS 1294	1090.75	-24.433	
SS 1293	1096	-25.09	
SS 2153	1102.75	-24.732	
SS 1291	1107.75	-24.893	
SS 2152	1118	-24.936	
SS 1290	1118.75	-25.783	0.1929
SS 1289	1161.5	-25.44	0.1334
SS 1288	1187	-24.819	6.7633
SS 1287	1197	-25.58	
SS 1283	1224	-27.115	0.3461
SS 1284	1229.75	-27.299	6.0082
SS 2150	1231.5	-28.934	19.226
SS 1282	1234	-27.84	3.6843
SS 1280	1244.5	-26.416	0.386
SS 1277	1286.5	-27.799	1.46
SS 1276	1289	-26.778	2.162
SS 1274	1301.5	-24.031	1.779
SS 1273	1311.5	-26.107	2.054
SS 1272	1316.5	-25.632	4.4364
SS 1271	1325.25	-26.434	2.08
SS 1270	1330.25	-25.659	16.85
SS 1269	1336.5	-26.562	2.8332
SS 1267	1344.75	-26.619	8.2654
SS 1264	1369	-26.815	2.5721
SS 1261	1386.5	-26.25	0.7676
SS 1260	1409	-26.556	6.6273
SS 1258	1420	-26.342	12.095
SS 2140	1429.5	-25.567	6.5329
SS 1256	1429.6	-26.425	5.3045
SS 2139	1437.75	-26.59	49.288
SS 1243	1541.75	-26.38	5.3013
SS 1240	1576	-26.11	2.9784
SS 1239	1584.5	-25.892	3.4751
SS 1238	1588.5	-26.04	3.0341
SS 1218	1676.5	-26.16	5.5509
SS 1221	1689	-26.38	2.4925
SS 1223	1711.5	-26.18	2.7151
SS 1224	1724	-26.68	0.7849
SS 1228	1805.75	-26.31	2.3542

GONZALES

Sample ID	depth(m)	e depth (ft)	e depth (m)	DC13	TOC
gonzales well-540	164.59	540	164.59	-26.08	0.2
gonzales well-590	179.83	590	179.83	-25.961	0.41
gonzales well-600	182.88	600	182.88	-25.824	0.62
gonzales well-610	185.93	610	185.93	-22.018	0.37
gonzales well-620	188.98	620	188.98	-24.853	3.1
gonzales well-630	192.02	630	192.02	-25.486	4.2
gonzales well-660	201.17	660	201.17	-23.821	3.44
gonzales well-680	207.26	680	207.26	-28.861	0.66
gonzales well-690	210.31	690	210.31	-25.45	6.82
gonzales well-700	213.36	700	213.36	-25.938	6.25
gonzales well-710	216.41	710	216.41	-25.774	4.34
gonzales well-720	219.46	720	219.46	-25.008	3.92
gonzales well-730	222.5	730	222.5	-26.003	2.66
gonzales well-750	228.6	750	228.6	-26.112	1.42
gonzales well-770	234.7	770	234.7	-26.725	0.93
gonzales well-790	240.79	790	240.79	-27.125	0.28
gonzales well-800	243.84	800	243.84	-26.977	0.31
gonzales well-830	252.98	830	252.98	-26.512	1.92
gonzales well-860	262.13	860	262.13	-26.81	0.43
gonzales well-890	271.27	890	271.27	-26.87	0.17
gonzales well-920	280.42	920	280.42	-26.117	0.19
gonzales well-950	289.56	950	289.56	-26.291	0.51
gonzales well-980	298.7	980	298.7	-27.091	0.33
gonzales well-101(	307.85	1010	307.85	-27.997	0.23
gonzales well-104(	316.99	1040	316.99	-26.998	0.26
gonzales well-107(	326.14	1070	326.14	-26.849	0.16
gonzales well-110(	335.28	1100	335.28	-25.872	0.18
gonzales well-113(	344.42	1130	344.42	-26.356	0.007
gonzales well-116(	353.57	1160	353.57	-24.75	0.1
gonzales well-119(	362.71	1190	362.71	-26.421	0.14
gonzales well-122(	371.86	1220	371.86	-26.622	0.47
gonzales well-125(	381	1250	381	-26.249	0.12
gonzales well-131(	399.29	1310	399.29	-26.045	0.18
gonzales well-134(	408.43	1340	408.43	-25.753	0.41
gonzales well-140(	426.72	1400	426.72	-26.067	0.74
gonzales well-146(	445.01	1460	445.01	-24.92	3.26
gonzales well-149(	454.15	1490	454.15	-21.206	11.24
gonzales outcrop	0.17	1144.02	348.7	-25.07	0.138
gonzales outcrop	0.37	1143.05	348.4	-25.369	0.116
gonzales outcrop	0.6	1141.93	348.06	-25.295	0.161
gonzales outcrop	0.72	1141.35	347.88	-24.857	0.151
gonzales outcrop	0.88	1140.56	347.64	-24.202	0.179
gonzales outcrop	1	1139.98	347.47	-25.521	0.168
gonzales outcrop	1.19	1139.06	347.19	-24.597	0.196
gonzales outcrop	1.41	1137.98	346.85	-24.247	0.215
gonzales outcrop	1.69	1136.62	346.44	-23.098	0.172
gonzales outcrop	1.78	1136.18	346.31	-25.047	0.149
gonzales outcrop	2.24	1133.94	345.62	-25.327	0.263
gonzales outcrop	2.85	1130.97	344.72	-25.965	0.266
gonzales outcrop	3.2	1129.25	344.19	-25.298	0.081
gonzales outcrop	7.55	1107.71	337.63	-25.982	0.053
gonzales outcrop	7.75	1106.71	337.33	-23.754	0.071
gonzales outcrop	7.79	1106.51	337.27	-24.1	0.046
gonzales outcrop	8.1	1104.99	336.8	-24.962	0.063
gonzales outcrop	27.8	1007.42	307.06	-26.676	0.089
gonzales outcrop	28.2	1005.44	306.46	-25.265	0.135
gonzales outcrop	28.5	1003.96	306.01	-23.667	0.142
gonzales outcrop	28.7	1002.97	305.7	-25.256	0.137
gonzales outcrop	80.3	747.43	227.82	-27.508	0.654
gonzales outcrop	80.6	745.94	227.36	-28.544	0.794
gonzales outcrop	80.88	744.57	226.94	-26.698	0.707
gonzales outcrop	81.29	742.53	226.32	-27.617	0.606
gonzales outcrop	81.8	740.01	225.55	-28.044	0.554
gonzales outcrop	82.2	738.02	224.95	-28.116	0.42
gonzales outcrop	83.1	733.56	223.59	-26.98	0.308
gonzales outcrop	83.5	731.58	222.99	-26.385	0.394
gonzales outcrop	84.1	729.16	222.25	-25.468	0.198
gonzales outcrop	84.7	727.38	221.7	-25.213	0.175
gonzales outcrop	85	726.49	221.43	-24.851	0.216
gonzales outcrop	85.4	725.3	221.07	-24.531	0.128
gonzales outcrop	85.7	724.4	220.8	-24.352	0.1
gonzales outcrop	86.1	723.21	220.43	-24.743	0.079
gonzales outcrop	86.4	722.32	220.16	-24.554	0.09
gonzales outcrop	86.7	721.42	219.89	-24.219	0.074
gonzales outcrop	87	720.53	219.62	-24.528	0.07
gonzales outcrop	87.3	719.63	219.34	-26.541	0.073
gonzales outcrop	87.4	719.33	219.25	-25.048	0.069
gonzales outcrop	87.7	718.44	218.98	-23.878	0.076
gonzales outcrop	88.1	717.25	218.62	-23.957	0.087
gonzales outcrop	88.3	716.65	218.44	-23.805	0.087
gonzales outcrop	88.4	716.35	218.34	-24.255	0.074
gonzales outcrop	88.9	714.86	217.89	-23.672	0.077
gonzales outcrop	89.3	713.67	217.53	-23.599	0.08
gonzales outcrop	89.6	712.78	217.26	-24.057	0.09
gonzales outcrop	89.7	712.48	217.17	-26.307	0.078
gonzales outcrop	89.8	712.18	217.07	-23.976	0.095
gonzales outcrop	92.5	704.14	214.62	-23.657	0.116
gonzales outcrop	93.7	700.57	213.53	-23.796	0.1
gonzales outcrop	94.4	698.48	212.9	-24.99	0.147
gonzales outcrop	94.5	698.18	212.81	-23.679	0.125
gonzales outcrop	94.6	697.88	212.71	-24.747	0.128
gonzales outcrop	94.7	697.58	212.62	-27.674	0.166
gonzales outcrop	94.8	697.29	212.53	-23.908	0.157
gonzales outcrop	94.9	696.99	212.44	-24.282	0.168
gonzales outcrop	95.6	694.91	211.81	-23.852	0.154
gonzales outcrop	95.7	694.61	211.72	-23.671	0.162
gonzales outcrop	95.8	694.31	211.63	-23.934	0.144
gonzales outcrop	96.2	693.12	211.26	-24.282	0.185
gonzales outcrop	96.5	692.23	210.99	-23.977	0.179
gonzales outcrop	96.9	691.04	210.63	-23.798	0.146
gonzales outcrop	96.9	691.04	210.63	-24.112	0.172
gonzales outcrop	96.9	691.04	210.63	-23.869	0.147
gonzales outcrop	97.7	688.65	209.9	-23.841	0.141
gonzales outcrop	98.1	687.46	209.54	-24.207	0.081
gonzales outcrop	98.4	686.57	209.27	-24.35	0.117
gonzales outcrop	98.8	685.37	208.9	-23.843	0.155
gonzales outcrop	100	681.8	207.81	-25.749	0.067
gonzales outcrop	101.5	677.33	206.45	-25.184	0.118
gonzales outcrop	104.9	667.2	203.36	-25.454	0.066
gonzales outcrop	113.1	642.78	195.92	-23.655	0.046
gonzales outcrop	134.6	578.72	176.39	-26.36	0.383
gonzales outcrop	135	577.53	176.03	-27.82	0.106
gonzales outcrop	135.15	577.08	175.89	-25.171	0.128
gonzales outcrop	135.2	576.93	175.85	-28.694	0.218
gonzales outcrop	135.6	575.76	175.5	-25.201	0.186
gonzales outcrop	135.6	575.75	175.49	-24.925	0.327
gonzales outcrop	135.7	575.45	175.4	-25.144	0.214
gonzales outcrop	136.48	573.12	174.69	-28.647	0.179
gonzales outcrop	136.5	573.07	174.67	-24.233	0.232
gonzales outcrop	136.55	572.91	174.62	-24.13	0.295
gonzales outcrop	137	571.57	174.21	-26.174	0.249
gonzales outcrop	137	571.57	174.21	-26.775	0.137
gonzales outcrop	137.2	570.98	174.03	-25.508	0.153
gonzales outcrop	137.7	569.49	173.58	-24.38	0.151
gonzales outcrop	137.85	569.04	173.44	-25.021	0.2
gonzales outcrop	138	568.59	173.31	-25.01	0.215

Table S5. Analytical data from the U-Pb CA-TIMS zircon analysis of the Riecito Mache Tuff.

							Radiogenic Isotope Ratios								Isotopic Ages					
Sample (a)	Th/U (b)	$^{206}Pb^*$ $\times 10^{-13}$ mol (c)	mol % $^{206}Pb^*$ (c)	Pb^*/Pb_c (c)	Pb_c (pg) (c)	$^{206}Pb/^{204}Pb$ (d)	$^{208}Pb/^{206}Pb$ (e)	$^{207}Pb/^{206}Pb$ (e)	% err (f)	$^{207}Pb/^{235}U$ (e)	% err (f)	$^{206}Pb/^{238}U$ (e)	% err (f)	corr. coef.	$^{207}Pb/^{206}Pb$ (g)	± (f)	$^{207}Pb/^{235}U$ (g)	± (f)	$^{206}Pb/^{238}U$ (g)	± (f)
z1	0.494	0.8933	99.63%	81	0.27	4989	0.159	0.047122	0.129	0.056884	0.196	0.008755	0.065	0.776	55.40	3.08	56.18	0.11	56.19	0.04
z2*	0.426	0.7152	99.40%	50	0.35	3122	0.137	0.047072	0.212	0.056731	0.258	0.008741	0.072	0.721	52.90	5.05	56.03	0.14	56.10	0.04
z3*	0.469	0.4306	99.26%	41	0.26	2528	0.150	0.047017	0.300	0.056654	0.352	0.008739	0.074	0.761	50.09	7.15	55.96	0.19	56.09	0.04
z5*	0.420	1.4577	99.74%	112	0.32	7064	0.134	0.047066	0.130	0.056751	0.183	0.008745	0.070	0.840	52.60	3.10	56.05	0.10	56.13	0.04
z6	0.335	2.3849	99.79%	141	0.41	8957	0.116	0.051418	0.208	0.074659	0.270	0.010531	0.139	0.651	259.60	4.78	73.11	0.19	67.53	0.09
z7*	0.440	2.5740	99.74%	116	0.54	7260	0.141	0.047141	0.113	0.056803	0.165	0.008739	0.071	0.839	56.40	2.69	56.10	0.09	56.09	0.04
z8	0.454	0.8794	99.60%	75	0.29	4697	0.145	0.047130	0.166	0.056869	0.214	0.008751	0.071	0.772	55.83	3.95	56.16	0.12	56.17	0.04
z9*	0.371	1.1111	99.63%	78	0.34	4999	0.119	0.047217	0.144	0.056857	0.194	0.008733	0.070	0.807	60.22	3.42	56.15	0.11	56.06	0.04
z11*	0.408	0.7796	99.40%	49	0.39	3087	0.131	0.047155	0.224	0.056820	0.270	0.008739	0.077	0.695	57.08	5.34	56.11	0.15	56.09	0.04
z12	0.476	0.8707	99.48%	58	0.37	3574	0.153	0.047245	0.176	0.057232	0.226	0.008786	0.073	0.764	61.61	4.20	56.51	0.12	56.39	0.04

(a) z1, z2, etc. are labels for analyses composed of single zircon grains that were annealed and chemically abraded (S32). Fraction labels with * denote analyses used in the weighted mean calculation.

(b) Model Th/U ratio calculated from radiogenic 208Pb/206Pb ratio and 207Pb/235U date.

(c) Pb* and Pbc are radiogenic and common Pb, respectively. mol % $^{206}Pb^*$ is with respect to radiogenic and blank Pb.

(d) Measured ratio corrected for spike and fractionation only. Fractionation correction is 0.15 ± 0.03 (1 sigma) %/amu (atomic mass unit) for single-collector Daly analyses, based on analysis of EARTHTIME 202Pb-205Pb tracer solution.

(e) Corrected for fractionation, spike, common Pb, and initial disequilibrium in 230Th/238U. Common Pb is assigned to procedural blank with composition of 206Pb/204Pb = 18.60 ± 0.80%; 207Pb/204Pb = 15.69 ± 0.32%; 208Pb/204Pb = 38.51 ± 0.74% (1 sigma). 206Pb/238U and 207Pb/206Pb ratios corrected for initial disequilibrium in 230Th/238U using Th/U [magma] = 3.

(f) Errors are 2 sigma, propagated using algorithms of Schmitz and Schoene (S35) and Crowley et al. (S36).

(g) Calculations based on the decay constants of Jaffey et al. (S24). 206Pb/238U and 207Pb/206Pb dates corrected for initial disequilibrium in 230Th/238U using Th/U [magma] = 3.

Table S6. Analytical data from the U-Pb LA-ICP-MS and CA-TIMS zircon analysis of the Riecito Mache Tuff.

sample name	238U 206Pb	1 sigma % error	207Pb 206Pb	1 sigma % error	206/238 age	1 sigma abs err	207/206 age	1 sigma abs err	Best age	1 sigma abs err Ma
B-110_50	129.9825	2.20%	0.0477	3.28%	49.4	1.1	252.3	69.7	49.4	1.1
B-110_49	127.7320	1.76%	0.0455	2.09%	50.3	0.9	0.0	24.1	50.3	0.9
B-110_48	124.9247	1.65%	0.0476	1.83%	51.4	0.8	43.9	41.7	51.4	0.8
B-110_47	124.0451	1.57%	0.0468	1.58%	51.8	0.8	39.5	39.9	51.8	0.8
B-110_46	123.3919	1.44%	0.0466	1.52%	52.0	0.7	28.9	38.5	52.0	0.7
B-110_45	123.3185	1.61%	0.0454	1.33%	52.1	0.8	0.0	0.0	52.1	0.8
B-110_44	122.2317	1.62%	0.0485	1.67%	52.5	0.8	158.1	38.5	52.5	0.8
B-110_43	121.1531	1.61%	0.0448	1.51%	53.0	0.8	0.0	0.0	53.0	0.8
B-110_42 *	**120.3530**	**1.81%**	**0.0475**	**2.27%**	**53.3**	**1.0**	**66.9**	**54.9**	**53.3**	**1.0**
B-110_41 *	**118.9386**	**1.45%**	**0.0474**	**1.55%**	**54.0**	**0.8**	**93.1**	**38.4**	**54.0**	**0.8** *
B-110_40 *	**117.9010**	**1.51%**	**0.0477**	**1.40%**	**54.4**	**0.8**	**83.4**	**34.4**	**54.4**	**0.8**
B-110_39 *	**115.5159**	**1.31%**	**0.0468**	**0.90%**	**55.6**	**0.7**	**73.2**	**27.8**	**55.6**	**0.7**
B-110_38 *	**115.4896**	**1.48%**	**0.0484**	**1.79%**	**55.6**	**0.8**	**146.8**	**43.8**	**55.6**	**0.8**
B-110_37 *	**115.0622**	**1.11%**	**0.0457**	**0.86%**	**55.8**	**0.6**	**0.0**	**15.9**	**55.8**	**0.6**
B-110_36 *	**115.0535**	**1.42%**	**0.0480**	**1.42%**	**55.8**	**0.8**	**99.0**	**35.9**	**55.8**	**0.8**
B-110_35 *	**115.0333**	**1.32%**	**0.0467**	**1.27%**	**55.8**	**0.7**	**39.4**	**33.4**	**55.8**	**0.7**
B-110_34 *	**115.0225**	**1.30%**	**0.0477**	**1.29%**	**55.8**	**0.7**	**167.1**	**32.5**	**55.8**	**0.7**
B-110_33 *	**114.9871**	**1.53%**	**0.0472**	**1.67%**	**55.8**	**0.9**	**73.8**	**43.2**	**55.8**	**0.9**
B-110_32 *	**114.9507**	**1.24%**	**0.0463**	**1.30%**	**55.8**	**0.7**	**63.0**	**33.7**	**55.8**	**0.7**
B-110_31 *	**114.4626**	**1.33%**	**0.0469**	**1.08%**	**56.1**	**0.7**	**61.0**	**31.3**	**56.1**	**0.7**
B-110_30 *	**114.3735**	**1.47%**	**0.0462**	**1.14%**	**56.1**	**0.8**	**17.8**	**30.9**	**56.1**	**0.8**
B-110_29 *	**114.3663**	**1.42%**	**0.0469**	**1.15%**	**56.1**	**0.8**	**87.0**	**31.2**	**56.1**	**0.8**
B-110_28 *	**113.8808**	**1.59%**	**0.0467**	**1.26%**	**56.4**	**0.9**	**31.5**	**31.7**	**56.4**	**0.9**
B-110_27 *	**113.5241**	**1.44%**	**0.0469**	**1.41%**	**56.5**	**0.8**	**99.6**	**34.3**	**56.5**	**0.8**
B-110_26 *	**111.8125**	**1.62%**	**0.0465**	**1.05%**	**57.4**	**0.9**	**23.9**	**28.3**	**57.4**	**0.9**
B-110_25 *	**109.7222**	**1.63%**	**0.0463**	**2.20%**	**58.5**	**0.9**	**162.2**	**59.3**	**58.5**	**0.9**
B-110_24	108.4996	1.69%	0.0513	1.70%	59.1	1.0	393.1	44.7	59.1	1.0
B-110_23	102.8870	1.71%	0.0486	1.73%	62.4	1.1	128.2	42.2	62.4	1.1
B-110_22	94.8850	2.15%	0.0531	2.61%	67.6	1.4	332.8	59.7	67.6	1.4
B-110_21	92.5295	1.26%	0.0477	1.21%	69.3	0.9	79.0	32.1	69.3	0.9
B-110_20	92.1185	1.49%	0.0455	1.47%	69.6	1.0	128.9	47.5	69.6	1.0
B-110_19	89.9886	2.01%	0.0483	2.53%	71.2	1.4	177.0	61.2	71.2	1.4
B-110_18	88.8842	1.92%	0.0445	2.02%	72.1	1.4	0.0	0.0	72.1	1.4
B-110_17	68.0999	1.52%	0.0492	1.81%	94.0	1.4	158.2	44.0	94.0	1.4
B-110_16	66.7055	1.30%	0.0474	1.15%	95.9	1.2	114.4	35.2	95.9	1.2
B-110_15	31.4134	1.05%	0.0502	0.63%	202.0	2.1	205.1	17.8	202.0	2.1
B-110_14	26.3220	1.12%	0.0505	0.76%	240.4	2.6	220.0	21.8	240.4	2.6
B-110_13	25.8561	3.29%	0.0520	3.32%	244.6	7.9	286.2	74.9	244.6	7.9
B-110_12	23.2769	1.30%	0.0518	0.66%	271.2	3.4	275.6	18.5	271.2	3.4
B-110_11	22.7715	1.21%	0.0592	1.03%	277.1	3.3	643.9	24.0	277.1	3.3
B-110_10	22.3345	1.63%	0.0520	1.63%	282.4	4.5	278.8	38.9	282.4	4.5
B-110_9	21.7107	1.18%	0.0526	0.67%	290.3	3.3	313.6	19.2	290.3	3.3
B-110_8	13.8995	1.03%	0.0560	0.54%	447.9	4.5	453.1	15.4	447.9	4.5
B-110_7	7.1388	1.88%	0.0740	0.80%	845.1	14.9	1030.1	19.4	845.1	14.9
B-110_6	7.0245	1.97%	0.0690	0.97%	858.0	15.8	900.8	21.9	858.0	15.8
B-110_5	5.9649	1.63%	0.0726	1.09%	999.1	15.0	1028.7	26.2	1028.7	26.2
B-110_4	5.1921	1.11%	0.0787	0.55%	1135.5	11.5	1166.6	15.7	1166.6	15.7
B-110_3	5.0852	1.14%	0.0788	0.59%	1157.3	12.1	1166.7	14.7	1166.7	14.7
B-110_2	5.3680	2.21%	0.0815	1.04%	1101.2	22.3	1256.4	24.3	1256.4	24.3

BOLD * = Analyzed accepted in the TUFFZIRC age calculation

U/Pb and 206Pb/ 207Pb fractionation is calibrated relative to fragments of a large Peixe zircon of 564 ± 4 Ma (2-sigma).

All uncertainties are reported at the 1-sigma level, and include only measurement errors. Systematic errors would increase age uncertainties by 1-2%.

Best age = $^{206}Pb/^{238}U$ for ages <1000 Ma and $^{206}Pb/^{207}Pb$ for ages >1000 Ma

Table S7. Mar2x DC13 isotopic composition (C) and Deuterium compositions (D) of n-alkanes with 25, 27, 29, and 31 carbon atoms. CPI=Carbon Preference Index

Depth (ft)	Depth (m)	CPI (ΣOdd(C25-C33)/ΣEven(C26-C34)	Average Chain Length	$\delta^{13}C_{25}$	$\delta^{13}C_{27}$	$\delta^{13}C_{29}$	$\delta^{13}C_{31}$	$\delta D_{n\text{-}C17}$	$\delta D_{n\text{-}C25}$	$\delta D_{n\text{-}C27}$	$\delta D_{n\text{-}C29}$	$\delta D_{n\text{-}C31}$
7181.10	2188.80	1.47	29.97	-30.49	-30.51	-30.60	-31.62			-167.15	-173.96	**-165.87**
7190.60	2191.69	1.50	30.05	-31.02	-30.75	-30.89	-31.72			-167.72	-174.63	**-170.55**
7253.11	2210.75	1.58	30.23	-30.27	-30.35	-30.47	-31.44		-164.08	-175.18	-174.96	**-166.25**
7262.00	2213.46	1.66	29.81	-30.69	-30.65	-30.55	-31.31		-159.42	-170.42	-170.74	**-164.69**
7273.00	2216.81	1.61	29.91	-31.17	-30.60	-31.09	-32.32		-129.23		-172.63	**-165.74**
7282.40	2219.68	1.49	29.85	-30.20	-29.90	-30.68	-31.44		-157.37	-164.97	-168.00	**-165.84**
7343.10	2238.18	1.61	29.81	-30.93	-30.47	-31.12	-32.30		-157.90	-164.16		
7403.00	2256.43	1.56	29.70	-30.66	-30.84	-31.16	-32.03		-166.98	-169.03	-171.25	**-166.50**
7409.90	2258.54	1.53	29.46	-31.10	-30.89	-31.22	-32.18		-154.26	-166.34	-167.93	**-165.64**
7428.60	2264.24	1.44	29.43	-31.22	-30.71	-31.22	-32.19		-160.06	-165.96	-168.44	
7446.30	2269.63											**-161.70**
7517.11	2291.22	1.58	30.00	-31.90	-31.86	-32.36	-33.38		-163.15	-168.62	-178.75	**-171.57**
7522.80	2292.95	1.56	29.79	-31.48	-32.25	-32.47	-33.53					**-174.77**
7533.60	2296.24	1.29	29.35	-31.50	-33.32	-32.44	-32.95					
7586.60	2312.40	1.42	29.60		-31.88	-31.88	-33.10	**-165.9**				**-152.90**
7599.70	2316.39	1.44	29.41	-30.49	-30.47	-30.46	-30.96		-165.71	-166.31	-167.71	**-163.43**
7602.10	2317.12	1.38	29.59	-29.88	-29.91	-30.10	-30.88	**-171.9**	-158.94	-163.68	-162.57	**-156.29**
7631.60	2326.11	1.60	28.28	-28.81	-29.35	-29.87	-30.60		-140.22	-140.79	-140.16	**-130.68**
7642.00	2329.28	1.55	29.62	-30.22	-30.87	-31.32	-32.27					**-143.54**
7787.70	2373.69	1.62	28.88	-29.25	-29.01	-29.50	-30.36		-148.74	-152.08	-159.05	**-148.25**
7848.40	2392.19	1.62	28.88	-29.47	-29.87	-30.42	-31.48		-122.14	-126.66	-130.17	**-130.11**
7989.20	2435.11							**-164.0**	-155.26	-151.75		**-133.74**

Table S8. Diversity summary results for Mar2x, Riecito Mache and Gonzales sites

N=number of pollen and spores counted per sample

S=number of species per sample

SD=Standing Diversity, after range-through method and excluding singletons,

numbers in red indicate samples with edge-effect that were excluded from standing diversity analysis

SI=Simpson Index (it was not calculated for samples with counts <80)

MAR 2x

depth(m)	depth (ft)	N	S	SD	SI	rarefaction (100 cutoff)
2080.931	6827.2	234	50	43	0.926	33.8408
2080.961	6827.3	231	46	64	0.91	28.71095
2082.698	6833	83	29	73	0.9	
2082.729	6833.1	180	53	92	0.899	36.88162
2085.228	6841.3	377	68	118	0.954	38.74392
2086.6	6845.8	43	15	120		
2088.49	6852	69	28	126		
2088.581	6852.3	97	36	133	0.918	
2089.495	6855.3	63	28	136		
2090.257	6857.8	270	49	143	0.922	30.03795
2090.867	6859.8	124	40	145	0.919	35.7173
2091.629	6862.3	27	12	145		
2099.249	6887.3	352	45	152	0.896	27.81719
2100.499	6891.4	53	22	153		
2100.743	6892.2	255	47	159	0.907	29.55577
2103.12	6900	201	56	173	0.908	37.84145
2103.272	6900.5	119	32	178	0.929	29.85761
2105.04	6906.3	120	30	181	0.777	27.31886
2106.839	6912.2	326	69	187	0.932	37.71406
2108.545	6917.8	261	48	192	0.932	32.31432
2109.033	6919.4	67	32	195		
2112.264	6930	21	15	196		
2112.508	6930.8	49	22	196		
2114.001	6935.7	190	41	197	0.943	31.92432
2116.623	6944.3	113	28	199	0.882	26.44123
2117.75	6948	204	48	204	0.93	36.26057
2119.122	6952.5	58	22	203		
2120.067	6955.6	22	9	203		
2122.322	6963	70	19	204		
2122.353	6963.1	158	31	208	0.93	26.58346
2123.572	6967.1	171	24	210	0.779	19.64622
2125.188	6972.4	36	18	212		
2125.98	6975	307	37	215	0.879	23.11023
2127.26	6979.2	269	39	216	0.904	26.62977
2128.754	6984.1	213	46	218	0.911	30.45631
2129.363	6986.1	208	47	221	0.907	30.5351
2129.394	6986.2	97	30	219	0.904	
2130.003	6988.2	405	54	220	0.929	31.82342
2131.405	6992.8	357	57	221	0.93	33.46974
2133.356	6999.2	79	32	217		
2137.44	7012.6	140	47	219	0.933	39.0969
2139.33	7018.8	222	46	215	0.944	34.27492
2141.068	7024.5	91	27	216	0.898	
2142.988	7030.8	293	49	218	0.908	30.5061
2145.426	7038.8	103	22	212	0.905	21.82351
2147.011	7044	74	29	212		
2149.206	7051.2	160	43	215	0.915	33.81731
2150.669	7056	56	31	217		
2151.949	7060.2	216	53	219	0.96	38.73695
2154.022	7067	75	29	218		
2154.906	7069.9	152	49	222	0.942	38.12485
2155.515	7071.9	91	30	221	0.924	
2156.094	7073.8	211	50	223	0.939	33.27213
2156.704	7075.8	88	23	224	0.789	
2159.142	7083.8	286	42	228	0.933	26.6515
2160.148	7087.1	124	34	230	0.897	30.67068
2161.245	7090.7	60	15	229		
2163.105	7096.8	175	36	230	0.85	27.34089
2163.47	7098	220	40	229	0.926	28.74915
2166.244	7107.1	34	13	228		
2167.86	7112.4	100	37	229	0.901	37
2168.561	7114.7	89	26	231	0.912	
2169.201	7116.8	224	45	231	0.909	32.43615
2169.566	7118	75	28	229		
2170.206	7120.1	328	58	234	0.916	33.3976
2170.877	7122.3	73	21	235		
2171.73	7125.1	173	42	235	0.91	31.05399
2173.254	7130.1	88	23	235	0.895	
2173.559	7131.1	247	14	237	0.39	8.65114
2176.059	7139.3	103	24	237	0.828	23.64819
2176.79	7141.7	79	28	237		
2177.186	7143	79	27	239		
2177.796	7145	256	60	240	0.921	35.61353
2178.893	7148.6	143	27	237	0.785	23.30385
2179.899	7151.9	139	52	239	0.94	43.24306
2180.539	7154	96	26	239	0.839	
2183.74	7164.5	245	52	239	0.914	33.88869
2185.446	7170.1	53	17	237		
2190.079	7185.3	77	40	238		
2193.127	7195.3	173	42	239	0.935	32.78966
2196.511	7206.4	305	65	236	0.944	38.77725
2205.38	7235.5	25	15	232		
2208.55	7245.9	69	30	233		
2225.131	7300.3	226	52	237	0.9	33.3652
2229.216	7313.7	310	69	238	0.904	35.64243
2235.434	7334.1	93	29	230	0.888	
2241.926	7355.4	148	33	232	0.911	28.35855
2248.357	7376.5	306	65	235	0.918	35.21873
2255.063	7398.5	272	53	235	0.923	32.34071
2261.128	7418.4	30	16	231		
2266.828	7437.1	260	63	234	0.948	37.99534
2266.859	7437.2	270	56	230	0.933	32.5353
2274.143	7461.1	127	34	225	0.89	30.00787
2277.77	7473	50	33	224		
2287.615	7505.3	226	69	220	0.919	41.80797
2290.938	7516.2	204	39	213	0.936	29.11651
2290.968	7516.3	217	38	212	0.934	30.00478
2292.187	7520.3	215	56	210	0.942	38.46391
2294.23	7527	299	41	207	0.931	26.63081
2294.961	7529.4	54	21	205		
2295.876	7532.4	28	13	204		
2305.111	7562.7	283	39	203	0.886	24.19845
2306.726	7568	127	26	200	0.842	22.74922
2308.921	7575.2	109	30	198	0.866	28.89358
2310.567	7580.6	114	33	201	0.902	30.74356
2311.146	7582.5	252	48	201	0.886	30.64614
2311.725	7584.4	287	46	196	0.91	27.84163
2312.975	7588.5	233	26	188	0.888	20.27
2314.773	7594.4	38	12	187		
2315.535	7596.9	129	28	187	0.891	24.90408
2315.87	7598	71	20	186		
2316.2	7599.08	185	38	186	0.922	29.12048
2316.876	7601.3	116	55	184	0.955	49.84964
2324.374	7625.9	46	20	176		
2324.74	7627.1	161	47	178	0.909	36.83015
2325.685	7630.2	103	29	175	0.926	28.59106
2325.953	7631.08	315	29	174	0.786	19.58383
2326.508	7632.9	144	39	174	0.909	31.57008
2328.702	7640.1	27	20	176		
2329.007	7641.1	195	44	180	0.904	30.15669
2331.08	7647.9	29	14	176		
2338.944	7673.7	355	19	176	0.453	9.74096
2339.066	7674.1	304	32	174	0.918	20.78607
2341.413	7681.8	40	7	169		
2342.175	7684.3	330	14	169	0.351	8.230623
2342.784	7686.3	343	20	167	0.607	11.96631
2343.211	7687.7	329	18	166	0.699	11.3128
2343.333	7688.1	387	24	165	0.502	12.37332
2343.363	7688.2	300	12	165	0.556	7.845778
2343.699	7689.3	73	5	165		
2343.973	7690.2	102	9	165	0.295	8.862745
2346.198	7697.5	64	10	165		
2346.381	7698.1	56	20	164		
2373.66	7787.6	296	21	163	0.409	10.38734
2373.843	7788.2	117	17	162	0.711	16.08192
2374.88	7791.6	42	17	159		
2376.983	7798.5	22	12	157		
2379.025	7805.2	60	28	156		
2380.183	7809	93	39	153	0.92	
2380.244	7809.2	42	27	148		
2380.488	7810	26	13	146		
2381.646	7813.8	57	27	145		
2384.237	7822.3	80	30	142		
2384.511	7823.2	25	11	136		
2386.919	7831.1	43	21	137		
2392.162	7848.3	143	21	135	0.766	18.77638
2392.528	7849.5	35	16	135		
2392.589	7849.7	96	36	132	0.908	
2392.741	7850.2	64	33	127		
2393.076	7851.3	73	21	123		
2407.768	7899.5	136	41	118	0.924	35.84985
2421.514	7944.6	215	46	118	0.911	30.2725
2423.008	7949.5	54	16	112		
2434.895	7988.5	154	33	111	0.901	26.78629
2435.687	7991.1	22	10	108		
2436.175	7992.7	144	31	107	0.893	25.77377
2437.12	7995.8	209	50	103	0.911	33.39706
2437.394	7996.7	145	44	93	0.948	37.09071
2437.729	7997.8	43	23	86		
2438.278	7999.6	75	22	80		
2438.888	8001.6	312	23	76	0.593	12.88582
2455.822	8057.16	120	44	68	0.92	38.85824
2468.118	8097.5	153	38	49	0.936	31.27015
2484.12	8150	245	28	31	0.904	18.95329
2492.654	8178	269	22	19	0.808	15.17833

Riecito Mache

depth(m)	N	S	SD	SI
1090.75	22	13	12	
1096	434	31	34	0.44
1096.1	515	44	48	0.71
1100.5	15	8	50	
1102.75	61	23	56	
1107.75	14	10	59	
1126.3	34	22	61	
1138.2	14	9	61	
1139.2	102	41	70	0.96
1152.9	275	30	75	0.9
1165	86	16	75	0.71
1197	70	27	76	
1203.7	33	13	75	
1204	23	15	78	
1204.5	28	11	77	
1205.6	73	25	79	
1229.75	552	40	88	0.56
1229.78	639	41	93	0.51
1229.79	166	21	96	0.69
1231.5	76	14	97	
1234	364	41	97	0.86
1234.5	34	11	97	
1235.5	17	10	98	
1236.5	17	11	97	
1244.5	76	36	99	
1245	62	21	96	
1246	39	10	94	
1253.8	69	20	94	
1254.7	26	13	95	
1256.3	63	18	94	
1259.2	13	7	93	
1259.4	110	45	93	0.96
1259.7	11	8	82	
1261	382	40	82	0.81
1262.5	22	11	77	
1276	30	12	75	
1281.5	41	13	74	
1286.5	90	31	75	0.94
1289	57	21	72	
1289.7	94	28	72	0.91
1289.8	128	39	71	0.92
1290.3	17	10	63	
1290.5	136	29	62	0.86
1290.8	68	13	55	
1292.3	297	14	52	0.21
1293.4	16	5	48	
1293.7	331	33	48	0.85
1294.1	49	8	39	
1295.4	46	13	39	
1295.45	109	36	34	0.91
1298.1	23	12	11	

Gonzales

depth (m)	depth (ft)	N	S	SI	tion (120 cutoff)
121.92	400	42	15		
164.33	539.13	62	24		
164.59	540	58	27		
173.31	568.59	141	41	0.91	37.66
173.58	569.49	47	21		
173.76	570.08	65	35		
175.12	574.56	80	26		
175.12	574.56	134	43	0.91	39.84
175.13	574.56	50	27		
175.49	575.75	43	23		
175.89	577.08	164	27	0.91	24.6
176.39	578.72	193	60	0.94	44.82
219.62	720.53	261	26	0.83	19.21
221.02	725.14	302	30	0.85	19.56
222.25	729.16	304	27	0.85	17.25
222.99	731.58	290	40	0.81	26.4
223.59	733.56	296	27	0.77	18.5
224.19	735.54	279	16	0.58	11.14
224.95	738.02	282	34	0.83	20.99
225.55	740.01	272	28	0.83	19.76
226.32	742.53	236	31	0.8	20.55
226.94	744.57	302	31	0.84	19.22
227.36	745.94	178	28	0.82	22.24
227.82	747.43	202	23	0.88	19.83
262.13	860	111	20	0.73	
271.27	890	78	12		
344.42	1130	41	15		
344.48	1130.2	142	12	0.7	11.07
344.72	1131	233	15	0.62	11.13
353.57	1160	62	14		
371.86	1220	79	17		
381	1250	44	14		
390.14	1280	83	19	0.71	
393.19	1290	176	15	0.32	11.8
408.43	1340	78	22		
435.86	1430	74	26		
445.01	1460	91	22	0.8	
454.15	1490	65	23		
463.3	1520	90	18	0.81	
472.44	1550	149	23	0.63	20.31
481.58	1580	92	17	0.64	
490.73	1610	101	18	0.7	
527.3	1730	218	18	0.44	13.38
536.45	1760	126	8	0.33	7.81
545.59	1790	124	13	0.28	12.71
554.74	1820	101	8	0.28	
563.88	1850	44	7		
582.17	1910	44	15		
600.46	1970	51	12		

Table S9. Relative abundances of dry vs wet indicator for Mar2x core. Precipitation preferences of families identified in this study are derived from Punyasena study (S79) of Gentry's 144-transect neotropical plant database.

Precipitation Preferences

Family	wet	dry
Arecaceae	1	
Olacaceae	1	
Araceae	1	
Annonaceae	1	
Ericaceae	1	
Moraceae	1	
Convolvulaceae	1	
Sapotaceae	1	
Passifloraceae	1	
Malvaceae	1	
Podocarpaceae	1	
Fabaceae		1
Euphorbiaceae		1
Proteaceae		1
Poaceae		1
Podocarpaceae		1
Ulmaceae		1
Myrtaceae		1
Onagraceae		1

Relative Abundance, MAR2x core

depth (m.)	depth (ft.)	wet (%)	dry (%)
2080.9	6827.2	59.4	2.6
2081	6827.3	58.4	1.3
2082.7	6833	37.3	0
2082.7	6833.1	46.1	2.2
2085.2	6841.3	48.5	2.7
2088.6	6852.3	38.1	3.1
2090.3	6857.8	59.6	1.5
2090.9	6859.8	68.5	0.8
2099.2	6887.3	70.7	1.7
2100.7	6892.2	52.5	0
2103.1	6900	38.8	1
2103.3	6900.5	60.5	5.9
2105	6906.3	57.5	3.3
2106.8	6912.2	47.9	1.2
2108.5	6917.8	54.4	1.5
2114	6935.7	59.5	0
2116.6	6944.3	50.4	0
2117.8	6948	48.5	0.5
2122.4	6963.1	72.2	1.3
2123.6	6967.1	82.5	0
2126	6975	82.7	0
2127.3	6979.2	78.4	2.6
2128.8	6984.1	50.2	4.2
2129.4	6986.1	56.3	1.9
2129.4	6986.2	74.2	3.1
2130	6988.2	66.4	4.7
2131.4	6992.8	59.7	0.8
2137.4	7012.6	53.6	0.7
2139.3	7018.8	32	5
2141.1	7024.5	60.4	2.2
2143	7030.8	59	0
2145.4	7038.8	55.3	1
2149.2	7051.2	45.6	2.5
2151.9	7060.2	47.7	5.6
2154.9	7069.9	51.3	3.9
2155.5	7071.9	70.3	2.2
2156.1	7073.8	47.9	3.3
2156.7	7075.8	76.1	1.1
2159.1	7083.8	74.5	1.4
2160.1	7087.1	65.3	4
2163.1	7096.8	68.6	2.9
2163.5	7098	60	0
2167.9	7112.4	49	5
2168.6	7114.7	46.1	4.5
2169.2	7116.8	61.2	3.1
2170.2	7120.1	73.8	1.2
2171.7	7125.1	67.1	2.9
2173.3	7130.1	65.9	2.3
2173.6	7131.1	100	0
2176.1	7139.3	78.6	1
2177.8	7145	67.6	7
2178.9	7148.6	76.2	1.4
2179.9	7151.9	69.1	3.6
2180.5	7154	72.9	1
2183.7	7164.5	73.1	3.3
2193.1	7195.3	45.7	3.5
2196.5	7206.4	64.6	2
2225.1	7300.3	44.7	2.2
2229.2	7313.7	72.9	1.9
2235.4	7334.1	67.7	7.5
2241.9	7355.4	67.6	0.7
2248.4	7376.5	71.6	4.2
2255.1	7398.5	63.6	1.8
2266.8	7437.1	46.2	2.3
2266.9	7437.2	50.7	2.6
2274.1	7461.1	63	2.4
2287.6	7505.3	58	3.5
2290.9	7516.2	67.2	1.5
2291	7516.3	65	0.5
2292.2	7520.3	54	2.3
2294.2	7527	54.2	0.7
2305.1	7562.7	83	0.7
2306.7	7568	73.2	0.8
2308.9	7575.2	56.9	5.5
2310.6	7580.6	51.8	4.4
2311.1	7582.5	73.4	0
2311.7	7584.4	73.9	1
2313	7588.5	62.7	0.4
2315.5	7596.9	75.2	1.6
2316.2	7599.08	49.7	0
2316.9	7601.3	57.8	0
2324.7	7627.1	52.2	0.6
2325.7	7630.2	50.5	3.9
2326	7631.08	62.2	3.5
2326.5	7632.9	63.9	0.7
2329	7641.1	9.2	0
2338.9	7673.7	96.3	0
2339.1	7674.1	48.7	0.3
2342.2	7684.3	98.2	0
2342.8	7686.3	96.5	0
2343.2	7687.7	97	0
2343.3	7688.1	95.9	0
2343.4	7688.2	91.7	0
2344	7690.2	96.1	0
2373.7	7787.6	81.8	0
2373.8	7788.2	29.1	3.4
2380.2	7809	47.3	1.1
2392.2	7848.3	84.6	0
2392.6	7849.7	28.1	0
2407.8	7899.5	42.6	1.5
2421.5	7944.6	52.6	0
2434.9	7988.5	41.6	0.6
2436.2	7992.7	74.3	0
2437.1	7995.8	62.2	0.5
2437.4	7996.7	40	2.1
2438.9	8001.6	93.9	0
2455.8	8057.16	47.5	1.7
2468.1	8097.5	29.4	0
2484.1	8150	77.6	0.4
2492.7	8178	86.2	0

2183.7	7164.5	73.1	3.3
2193.1	7195.3	45.7	3.5
2196.5	7206.4	64.6	2
2225.1	7300.3	44.7	2.2
2229.2	7313.7	72.9	1.9
2235.4	7334.1	67.7	7.5
2241.9	7355.4	67.6	0.7
2248.4	7376.5	71.6	4.2
2255.1	7398.5	63.6	1.8
2266.8	7437.1	46.2	2.3
2266.9	7437.2	50.7	2.6
2274.1	7461.1	63	2.4
2287.6	7505.3	58	3.5
2290.9	7516.2	67.2	1.5
2291	7516.3	65	0.5
2292.2	7520.3	54	2.3
2294.2	7527	54.2	0.7
2305.1	7562.7	83	0.7
2306.7	7568	73.2	0.8
2308.9	7575.2	56.9	5.5
2310.6	7580.6	51.8	4.4
2311.1	7582.5	73.4	0
2311.7	7584.4	73.9	1
2313	7588.5	62.7	0.4
2315.5	7596.9	75.2	1.6
2316.2	7599.08	49.7	0
2316.9	7601.3	57.8	0
2324.7	7627.1	52.2	0.6
2325.7	7630.2	50.5	3.9
2326	7631.08	62.2	3.5
2326.5	7632.9	63.9	0.7
2329	7641.1	9.2	0
2338.9	7673.7	96.3	0
2339.1	7674.1	48.7	0.3
2342.2	7684.3	98.2	0
2342.8	7686.3	96.5	0
2343.2	7687.7	97	0
2343.3	7688.1	95.9	0
2343.4	7688.2	91.7	0
2344	7690.2	96.1	0
2373.7	7787.6	81.8	0
2373.8	7788.2	29.1	3.4
2380.2	7809	47.3	1.1
2392.2	7848.3	84.6	0
2392.6	7849.7	28.1	0
2407.8	7899.5	42.6	1.5
2421.5	7944.6	52.6	0
2434.9	7988.5	41.6	0.6
2436.2	7992.7	74.3	0
2437.1	7995.8	62.2	0.5
2437.4	7996.7	40	2.1
2438.9	8001.6	93.9	0
2455.8	8057.16	47.5	1.7
2468.1	8097.5	29.4	0
2484.1	8150	77.6	0.4
2492.7	8178	86.2	0

Table S10. P2 core TEX86 values, BIT indices and SST estimates following the calibration of Kim et al (S85) and Liu et al (S86).
One standard deviation for the temperature estimation is 3.6 C (using Liu calibration (S86))

Elevation (m)	Age	TEX86	BIT	SST (Kim et al.)	SST (Liu et al.)
123	Late Paleocene	0.71	0	28.6	27.6
129.9	Late Paleocene	0.7	0	28.0	27.2
157	Late Paleocene	0.68	0.05	27.1	26.4
181.25	Late Paleocene	0.65	0	26.0	25.5
189.36	Late Paleocene	0.69	0	27.6	26.8
229.86	Late Paleocene	0.68	0	27.1	26.5
238	Late Paleocene	0.78	0	31.3	29.6
277.5	Late Paleocene	0.71	0	28.3	27.3
292.78	Late Paleocene	0.71	0.05	28.5	27.5
301.95	Late Paleocene	0.71	0.05	28.6	27.6
309.62	Late Paleocene	0.73	0	29.4	28.2
316.62	Early Eocene	0.75	0.05	30.0	28.6
336.4	Early Eocene	0.75	0.1	29.9	28.6
359.24	Early Eocene	0.79	0.12	31.8	29.9
372.74	Early Eocene	0.7	0.06	27.9	27.1
390.29	Early Eocene	0.83	0.09	33.0	30.8
404.3	Early Eocene	0.87	0.11	34.4	31.6
424.1	Early Eocene	0.84	0.13	33.5	31.1